Author Manuscript

Author Manuscript

Author Manuscript

Author Manuscript

HHS Public Access

Author manuscript

Curr Biol. Author manuscript; available in PMC 2018 June 05.

Published in final edited form as:

Curr Biol. 2017 June 05; 27(11): 1561–1572.e8. doi:10.1016/j.cub.2017.04.051.

Modular segregation of structural brain networks supports the development of executive function in youth

Graham L. Baum[a], **Rastko Ciric**[a], **David R. Roalf**[a], **Richard F. Betzel**[b], **Tyler M. Moore**[a], **Russell T. Shinohara**[c], **Ari E. Kahn**[b], **Simon N. Vandekar**[c], **Petra E. Rupert**[a], **Megan Quarmley**[a], **Philip A. Cook**[d], **Mark A. Elliott**[d], **Kosha Ruparel**[a], **Raquel E. Gur**[a], **Ruben C. Gur**[a], **Danielle S. Bassett**[b,e,†], and **Theodore D. Satterthwaite**[a,†,*]

[a]Department of Psychiatry of the University of Pennsylvania, Philadelphia, PA 19104 USA

[b]Department of Bioengineering of the University of Pennsylvania, Philadelphia, PA 19104 USA

[c]Department of Biostatistics and Epidemiology of the University of Pennsylvania, Philadelphia, PA 19104 USA

[d]Department of Radiology of the University of Pennsylvania, Philadelphia, PA 19104 USA

[e]Electrical and Systems Engineering of the University of Pennsylvania, Philadelphia, PA 19104 USA

SUMMARY

The human brain is organized into large-scale functional modules that have been shown to evolve in childhood and adolescence. However, it remains unknown whether the underlying white matter architecture is similarly refined during development, potentially allowing for improvements in executive function. In a sample of 882 participants (ages 8–22) who underwent diffusion imaging as part of the Philadelphia Neurodevelopmental Cohort, we demonstrate that structural network modules become more segregated with age, with weaker connections between modules and stronger connections within modules. Evolving modular topology facilitates global network efficiency, and is driven by age-related strengthening of hub edges present both within and between modules. Critically, both modular segregation and network efficiency are associated with enhanced executive performance, and mediate the improvement of executive functioning with age. Together, results delineate a process of structural network maturation that supports executive function in youth.

Graphical abstract

Address correspondence to: sattertt@mail.med.upenn.edu.
†= Co-senior authors
*= Lead contact

Publisher's Disclaimer: This is a PDF file of an unedited manuscript that has been accepted for publication. As a service to our customers we are providing this early version of the manuscript. The manuscript will undergo copyediting, typesetting, and review of the resulting proof before it is published in its final citable form. Please note that during the production process errors may be discovered which could affect the content, and all legal disclaimers that apply to the journal pertain.

AUTHOR CONTRIBUTIONS

Conceptualization: T.D.S, D.S.B. and G.L.B.; Methodology: D.S.B, T.D.S., G.L.B., R.C., D.R.R., R.F.B., T.M.M., R.T.S., A.E.K., S.N.V., P.E.R., M.Q., P.A.C. and M.A.E.; Investigation and Resources: R.E.G., R.C.G., K.R. and T.D.S; Writing: G.L.B., T.D.S. and D.S.B.; Editing and Revision: all authors; Supervision: T.D.S. and D.S.B.

Author Manuscript
Author Manuscript
Author Manuscript
Author Manuscript

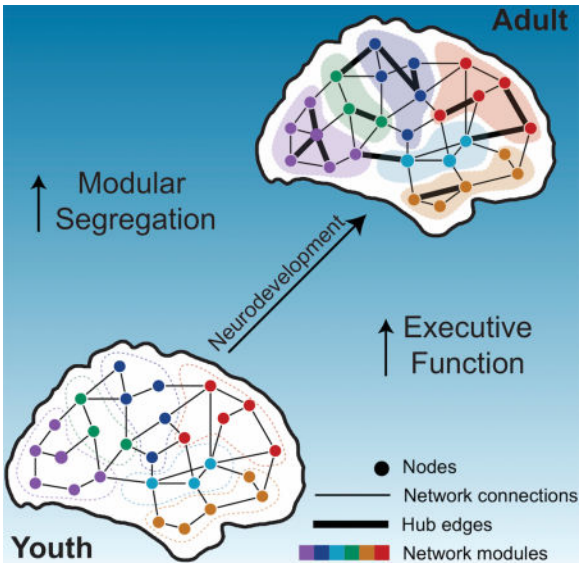

INTRODUCTION

Modularity is a fundamental feature of complex systems, including social groups, cyber-physical systems, and diverse biological networks [1]. A network module is a group of densely interconnected nodes, which often are the basis for specialized subunits of information processing [2]. Functional neuroimaging studies have demonstrated that the human brain has a well-defined modular organization, as reflected in the presence of large-scale functional networks [3–6]. While the exact number and spatial distribution of functional network modules varies somewhat by analytic approach, a remarkable convergence exists across independent datasets and laboratories [4–6].

Commonly described modules include somatomotor, visual, default mode, and frontoparietal control systems [5,6]. While brain network modules emerge very early in life [7], a growing body of work has shown that these functional modules are refined during youth. During childhood and adolescence, functional modules become more distinct: connectivity within modules increases while connectivity between modules declines [8–11]. Such development allows for functional specialization, reducing interference among systems and facilitating cognitive performance [12]. Modularity is particularly relevant for executive function, which relies on co-activation of executive regions and reciprocal suppression of non-executive regions such as the default mode network [13]. Thus, available data suggests that development of network modularity may serve as a substrate for the evolution of executive capability during youth.

Despite convergent evidence for the developmental emergence of functional network modularity, there is relatively scant data regarding the maturation of underlying structural brain networks that support this functional architecture [14]. Prior work demonstrates substantial correspondence between functional and structural measures of brain connectivity [15–17], although structural connections tend to be a subset of densely connected, polysynaptic functional networks [18]. Structural networks in adults are highly modular

Author Manuscript Author Manuscript Author Manuscript Author Manuscript

[19,20], but it remains unknown if this topology evolves substantially during youth. Correspondence between functional and structural data intuitively suggests that, like functional networks, structural networks should become increasingly segregated during development. However, prior studies using relatively small samples report conflicting results, including declining modularity [21], increasing modularity [22], or no change with age [23,24]. Larger sample sizes may be necessary for resolving the variability of findings reported in previous studies.

Beyond this mixed data regarding normative developmental trends, the impact of structural network development on cognitive performance remains poorly described. Cognitive capability improves substantially during youth, with executive function undergoing a protracted phase of development throughout adolescence and young adulthood [25]. Describing how underlying white matter architecture evolves to support executive function is necessary to understand the basis for many sources of adolescent morbidity and mortality, which are prominently associated with failures of executive function [26]. Finally, such data are a prerequisite for studies of neuropsychiatric disorders, which are increasingly understood as disorders of brain development [27], are marked by executive dysfunction [28], and are linked to the disruption of evolving network topology [29–31].

Here we sought to define the normative development of structural network modules, and delineate the impact of modular maturation on executive functioning. We tested the hypothesis that modules within structural brain networks become more segregated with age, as seen in functional brain networks. Further, we predicted that segregated structural modules would support enhanced executive functioning. To address these hypotheses, we capitalized upon a large sample of 882 youths who completed diffusion imaging as part of the Philadelphia Neurodevelopmental Cohort (PNC), a community-based study of brain development that includes rich neuroimaging and cognitive data [32]. As described below, results provide novel evidence that structural brain networks undergo a process of modular segregation analogous to prior accounts of functional network development. Critically, these data reveal that the refinement of structural network modules mediate the development of executive function.

RESULTS

We investigated the evolution of structural brain networks in a sample of 882 youth aged 8–22 who completed neuroimaging as part of the PNC (Figure 1A). As expected, executive function improved markedly with age ($p<1\times10^{-10}$, Figure 1B). Structural brain networks were constructed using nodes defined based on a parcellation of each subject's structural image into 234 anatomically defined regions [33]; structural connectivity between these nodes was estimated using deterministic tractography (Figure 2). Each network node was assigned *a priori* to one of the functional network modules defined by Yeo et al. [6]. Although these module partitions were defined in an independent dataset, using a different imaging modality, the modularity quality of the functional partition imposed on subject-level structural connectivity matrices (Q_{Yeo}) was highly significant ($p<1\times10^{-10}$). Furthermore, data-driven analysis of structural networks using community detection procedures [34–36]

Author Manuscript Author Manuscript Author Manuscript Author Manuscript

identified network modules that showed significant similarity to the *a priori* functional modules ($p<1\times10^{-10}$; see Figures S1 and S2).

Segregation of structural network modules increases with age

We first sought to understand whether structural network modules became more segregated with age. To do this, we calculated the average participation coefficient for each subject's network. The participation coefficient quantifies the relative balance of a brain region's between-module versus within-module connectivity: regions with a high participation coefficient (approaching the maximum value of 1) have strong between-module connectivity and weak within-module connectivity, while regions with lower participation coefficient values (approaching the minimum value of 0) have relatively weak between-module connectivity and strong within-module connectivity [37]. Greater modular segregation is therefore indicated by lower participation coefficient values, with reduced between-module and elevated within-module connectivity. We examined the development of modular segregation using a generalized additive model with penalized splines, which allows for statistically rigorous modeling of both linear and non-linear effects while minimizing over-fitting [38]. To ensure that results reflected changes in network topology rather than global differences in network connectivity, total network strength was also included as a covariate in all analyses [39], as was participant sex and in-scanner motion (see also below).

The participation coefficient declined significantly with age (Figure 3A; $p<1\times10^{-10}$), indicating enhanced modular segregation. While we report non-linear age effects throughout this study, we also estimated the effect size of the linear age effect on mean participation coefficient while controlling for age^2, sex, motion, and total network strength ($t=-0.31$, $p<1\times10^{-10}$). Notably, random resampling procedures provided striking evidence of a high degree of replicability of these observed developmental effects: all 10,000 sub-samples of 441 randomly-selected participants demonstrated significant modular segregation with age, while no subsamples with permuted data showed this effect (see Figure S3). Age-related increases in modular segregation were greatest during childhood and adolescence, and leveled off in early adulthood (Table S1). Developmental increases in modular segregation were differentially distributed across modules (Figure 3B), with the most robust declines observed in the somatomotor and default mode modules. To further understand which regions were driving these effects, we examined the participation coefficient of individual network nodes. As expected, the nodal participation coefficient declined in many regions (Figure 3C), with many of the most significant reductions occurring in regions within the default mode system. Two exceptions to this overall trend were observed, with increasing participation coefficient in the right rostral frontal gyrus and frontal operculum.

Next, we investigated the degree to which developmental effects on modular segregation were driven by changes in within-module connectivity, between-module connectivity, or both. We found that both effects were significant: within-module connectivity increased with age (Figure 4A; $p<1\times10^{-10}$), whereas between-module connectivity declined (Figure 4B; $p<1\times10^{-10}$). Moreover, modular segregation was reflected in individual network edges (Figure 4C), with permutation-based analysis revealing that a higher proportion of connections that strengthened with age were located within a module (Figure 4D; $p<0.001$).

Author Manuscript Author Manuscript Author Manuscript Author Manuscript

Results are robust to methodological approach and potential confounding variables

Given this strong evidence for developmental modular segregation, we next pursued an extensive set of supplementary analyses to determine if our results were dependent upon specific methodological choices. First, we evaluated alternative network partitions and measures of network segregation, to ensure that results were not specific to the functionally-defined partition used in the main analyses. Notably, the participation coefficient of a data-driven partition of the structural connectivity data yielded very similar results (Figure 5B; $p<1\times10^{-10}$; see also Figure S4). To ensure that developmental effects on modular segregation were not driven by age-related changes in modular composition, we also defined representative data-driven partitions for three age groups (childhood, adolescence, and early adulthood) and found remarkably high partition similarity across groups (Figure S5; see STAR Methods). We also measured the modularity quality index (Q) of network partitions, which quantifies how well a given partition maximizes the strength of within-module connections relative to a specified null model [1]. Higher Q values indicate that modules are highly segregated within a network. Convergent results were obtained when evaluating either the modularity quality of the Yeo et al. partition [6] (Q_{Yeo}) applied to each subject's data (Figure 5A; $p=1.06\times10^{-9}$), or by calculating the modularity quality of subject-specific partitions (Q_{subj}; Figure 5C; $p=0.0007$).

Second, we examined the impact of alternative network node definitions, edge measures, and edge normalization. Use of a more fine-grained network parcellation (N=463 nodes) did not impact the observed results, with age-related declines in the participation coefficient remaining highly significant (Figure 5D; $p<1\times10^{-10}$). Similarly, different measures of structural connectivity including streamline count (Figure 5E; $p=6.52\times10^{-7}$) and volume-normalized streamline density (Figure 5F; $p=4.56\times10^{-8}$) produced highly similar results. Additional analyses revealed that results were not driven by the potentially artifactual strengthening of short-range connections (Figure S6). Normalizing edges by total network strength (rather than including it as model covariate) also yielded similar results ($p<1\times10^{-10}$).

Third, we observed highly convergent results after applying multi-compartment diffusion modeling and probabilistic tractography, which may enhance sensitivity for detecting crossing fibers [40]. After constructing thresholded networks across a wide density range for each subject, we observed a significant age-related decrease in the integrated mean participation coefficient when edge weights in probabilistic connectivity matrices were defined by the inter-regional streamline count (Figure 5G; $p=7.24\times10^{-7}$), volume-normalized streamline count (Figure 5H; $p=2.98\times10^{-8}$), and the inter-regional connectivity probability (Figure 5I; $p=4.25\times10^{-7}$).

Fourth, to evaluate the influence of other potentially confounding variables, we also included total brain volume, handedness, race, and maternal education as model covariates; age effects on modular segregation remained significant ($p<1\times10^{-10}$). Similarly, results were unchanged when white matter volume ($p<1\times10^{-10}$) or mean white matter fractional anisotropy ($p<1\times10^{-10}$) were added as covariates. Conversely, results also remained consistent when all covariates were removed from the model ($p<1\times10^{-10}$).

Author Manuscript Author Manuscript Author Manuscript Author Manuscript

Fifth and finally, we evaluated the potential confounding influence of motion artifact [41]. Notably, all data included in this study passed a rigorous quality assurance procedure [42] and all high motion scans were excluded. Nevertheless, motion was associated with higher mean participation coefficient (p=6.08 × 10^{-7}). Accordingly, all analyses described therefore included in-scanner motion as a covariate. However, to ensure that developmental effects on modular segregation were not driven by age-related differences in head motion, analysis in a very low motion sub-sample (where motion was unrelated to age or participation coefficient) produced highly similar results (p<1×10^{-10}; Figure S7).

Modular segregation contributes to global network efficiency

Having established that network modules become more segregated with age, and that this finding was not dependent on specific analytic choices, we evaluated the impact of evolving network modularity on measures of global communication efficiency. Global network efficiency provides a measure of network integration by quantifying information flow across a network as the shortest path between pairs of nodes [43]. In many networks, modularity and global efficiency are inversely related, as a highly modular topology could require long communication paths to integrate information across the network. However, in some cases it is possible for networks to become both more modular *and* more efficient; this unusual situation occurs when connectivity within modules is efficiently organized and hub edges form strong links between otherwise segregated modules [2,44]. To determine which scenario characterized human neurodevelopment, we first examined the relationship between global efficiency and age while controlling for the covariates described previously. Replicating previous reports [21,23], we found that global efficiency increases with age (Figure 6A; p<1×10^{-10}). Next, we calculated the correlation between modular segregation (mean participation coefficient) and global efficiency, while co-varying for age to control for shared developmental trends. Mean participation coefficient was negatively associated with global efficiency (Figure 6B; p<1×10^{-10}), suggesting that the development of network modules does not result in fragmentation, but rather is associated with global network integration.

Age effects are concentrated in hub edges that promote network modularity and efficiency

To better understand this highly specialized association between network modularity and global efficiency, we evaluated the edge betweenness centrality for each network connection. Edge betweenness identifies hub connections by providing a measure of how much a given network edge lies upon the shortest path of communication through a network, and thus contributes to global efficiency [45]. Here we defined *hub edges* as those connections within the top quartile of edge betweenness across all network edges. Critically, edges that strengthened with age were enriched for hub edges (p<0.001; Figure 6C). Both within- (p<0.001) and between-module (p<0.001) edges that strengthened with age had higher betweenness than expected by chance (Figure 6D). Furthermore, the average strength of all within-module (Figure 6E; p<1×10^{-10}) and between-module (Figure 6F; p<1×10^{-10}) edges that strengthen with age was associated with global efficiency, suggesting that developmental effects are concentrated within connections that facilitate network integration. The striking combination of increasing modular segregation and enhanced global efficiency demonstrates that structural brain networks become both more modular and

Author Manuscript Author Manuscript Author Manuscript Author Manuscript

more integrated in development. These dual processes are driven by selective strengthening of network hub edges, which are present within network modules and also provide critical links between increasingly segregated modules.

Modular segregation mediates development of executive function in youth

Next, we evaluated the cognitive implications of modular segregation by examining associations with individual differences in executive function. Mean whole-brain participation coefficient was associated with improved executive performance (p=0.018). At the level of individual modules, we found that segregation of the frontoparietal control system was uniquely associated with executive ability (Figure 7A; p=0.005), suggesting a network-specific substrate for executive function. As a final step, we examined whether age-related changes in executive function and modularity were related. Mediation analyses revealed that this was indeed the case (Figure 7B; p=0.006), suggesting that the development of segregated structural brain modules mediates the age-related improvement in executive function. These mediating effects were specifically driven by the frontoparietal module (p=0.012). Similarly, global efficiency was associated with executive functioning (p=0.037), and also mediated executive development (p=0.002).

To evaluate the specificity of these results, we examined associations with other domains of cognition, such as social cognition and memory performance. While no association with memory was found, modular segregation was also significantly associated with social cognition (p=0.022), which was driven by segregation of the default mode module (p=0.012). Further, segregation of the default network mediated age-related improvements in social cognition (p=0.008). Together, these results demonstrate that developmental segregation of specific structural network modules may support the development of disparate cognitive domains.

DISCUSSION

Capitalizing on a large sample of youth imaged as part of the PNC, we demonstrated that modules within human structural brain networks become increasingly segregated with age. This result was robust to specific methodological choices, and driven by a combination of enhanced within-module connectivity and declining between-module connectivity. Age related changes were concentrated within specific hub edges, allowing for networks to simultaneously become more modular and more globally integrated with age. Critically, segregation of network modules mediated the development of executive function during adolescence.

The delineation of robust, reproducible large-scale functional networks has had a tremendous impact on human neuroscience research [5,6]. As a result, functional network modules have evolved to become the dominant framework by which human imaging data is interpreted. The conceptualization of the brain as a modular entity has had a particularly pronounced effect on theories of development, where convergent results have shown that functional network modules are present early in life [7], and continue to develop during youth [8–11]. In contrast, smaller studies of structural brain networks have produced heterogeneous results regarding the development of structural network modules that have not

Author Manuscript Author Manuscript Author Manuscript Author Manuscript

aligned well with functional imaging data [21,22,24]. When considered in light of prior studies that have reported substantial correspondence between brain structure and function [15–18], the disparity between developmental accounts of structural and functional network modules has been difficult to reconcile.

Leveraging a large sample imaged as part of the PNC, we were able to resolve this discrepancy by demonstrating that structural network modules develop in a similar manner as functional brain networks, and become increasingly segregated with age. Modular segregation was present at every scale evaluated, including the whole network, individual network modules, and specific network nodes. In contrast to the widespread regional pattern of modular segregation, the right frontal operculum and rostral middle frontal cortex became more integrated across development. These regions may increasingly serve as integrative hubs in the ventral attention (cingulo-opercular) and default mode networks [46]. Importantly, results were consistent across tractography methods and a variety of definitions for network nodes, edges, and modules; such methodological replication is critical as parameter choices may sometimes impact inference [47].

In many networks, modular segregation is associated with reduced capacity for global communication. We found that this was not the case in development, and that increasing modularity was in fact associated with enhanced network efficiency. This robust association was the result of targeted strengthening of hub edges. These hub edges were present within but also between modules, allowing for integration across increasingly segregated networks. These results accord with prior studies that have demonstrated that connections between network hubs strengthen preferentially with age [48], and that network efficiency increases during development [21,23]. The present data emphasize that increasing modular segregation does not result in isolation of functional sub-systems, but is associated with global network integration through strengthening of hub edges that facilitate both intra- and inter-module connectivity.

Having defined a normative process of modular segregation, we evaluated the cognitive impact of this developmental effect. While controlling for age, we found that greater modular segregation of structural brain networks was associated with better executive performance. Critically, modular segregation mediated the observed improvement of executive performance with age, and was driven by segregation of the frontoparietal module. Associations between module segregation and cognition were domain-specific: segregation of the default mode mediated age-related improvements in social cognition, which is reliant on regions within that network [49]. The process of structural network segregation may allow for functional specialization, and reduce competitive interference between brain systems [50]. Furthermore, building on prior work that reported an association between intelligence and the global efficiency of structural and functional networks in relatively small adult samples, we found that global efficiency also mediated developmental improvements in executive function. Taken together, the current data suggest that structural brain networks re-configure with age, becoming both more modular and more globally integrated. This specific topology may allow for both functional specialization within modules as well as coordination across modules, which is necessary for effective implementation of dynamic executive processes [44,50–52].

Author Manuscript Author Manuscript Author Manuscript Author Manuscript

Notwithstanding the strengths of this study, several limitations should be noted. First, this is a cross-sectional dataset, which has inherent limitations for studies of development [53]. The mediating role that network maturation plays in the development of executive function could be further interrogated using longitudinal data. These limitations offer clear directions for additional research. Ongoing follow-up of this cohort will yield informative data, as will other large-scale studies of brain development, including the IMAGEN consortium [54], the NKI-Rockland sample [55], and the forthcoming Adolescent Brain and Cognitive Development Study. Finally, it should be noted that diffusion-based tractography methods remain limited in their ability to fully resolve complex white matter trajectories in the human brain [56]. We attempted to overcome the tradeoff between connectome specificity and sensitivity [57,58] by replicating results using both tensor-based deterministic tractography and Bayesian probabilistic tractography procedures.

In summary, we demonstrated that structural brain modules become more segregated with age. Strengthening of specific within- and between-module hub edges allowed for a simultaneous process of network integration that evolves in concert with modular segregation. Finally, both modular segregation and global network efficiency mediated the development of executive function in youth. These data resolve an ongoing debate in the field regarding the normative development of structural brain networks, and delineate an important new mechanism for the development of executive functioning in youth. These findings may be relevant for understanding how individual differences in brain development associate with risk-taking behaviors, which are linked to failures of executive function, and are a major source of morbidity and mortality in adolescence [26]. Furthermore, as both abnormalities within developing networks and executive system dysfunction [28] are a common feature of diverse types of psychopathology [29–31], structural network development may evolve to become an important imaging biomarker of risk and resilience during the critical period of adolescence.

CONTACT FOR REAGENT AND RESOURCE SHARING

Further information and requests regarding resource sharing may be directed to the corresponding author (Theodore D. Satterthwaite; sattertt@mail.med.upenn.edu).

EXPERIMENTAL MODEL AND SUBJECT DETAILS

Participants—Diffusion tensor imaging (DTI) datasets were acquired as part of the Philadelphia Neurodevelopmental Cohort (PNC), a large community-based study of brain development. In total, 1601 subjects completed the cross-sectional neuroimaging protocol [32]. Datasets from 244 individuals were considered unusable due to lack of a complete diffusion scan (n=224), or incidental findings (n=20). The remaining 1357 participants underwent a rigorous manual and automated quality assurance protocol for DTI datasets [42], which excluded 157 subjects for poor data quality (e.g., low temporal signal-to-noise ratio). Of the remaining 1210 participants, 93 were excluded for low quality or incomplete FreeSurfer reconstruction of T1-weighted images. Of the remaining 1117 participants, 235 subjects were excluded for meeting any of the following criteria: gross radiological abnormalities, history of medical problems that might affect brain function, history of inpatient psychiatric hospitalization, use of psychotropic medication at the time of data

Author Manuscript Author Manuscript Author Manuscript Author Manuscript

acquisition, and/or high levels of in-scanner head motion during the DTI scan (mean relative displacement between non-weighted volumes > 2mm), which has been shown to impact measures derived from diffusion-weighted imaging [41,42]. These exclusions produced a final sample consisting of 882 youths (mean age=15.06, SD=3.15; 389 males, 493 females). Study procedures were approved by the Institutional Review Board of the Children's Hospital of Philadelphia and the Brain Behavior Laboratory at the University of Pennsylvania. All adult participants provided informed consent; all minors provided assent and their parent or guardian provided informed consent.

Cognitive assessment—The Penn computerized neurocognitive battery (Penn CNB) was administered to all participants. The CNB consists of 14 tests adapted from tasks applied in functional neuroimaging to evaluate a broad range of cognitive domains [25]. These domains include executive control (abstraction and flexibility, attention, working memory), episodic memory (verbal, facial, spatial), complex cognition (verbal reasoning, nonverbal reasoning, spatial processing), social cognition (emotion identification, emotion intensity differentiation, age differentiation) and sensorimotor and motor speed. Accuracy and speed for each test were *z*-transformed. Cognitive performance was summarized by a recent factor analysis of both speed and accuracy data [59], which delineated three factors corresponding to the efficiency of executive function, episodic memory, and social cognition. Two participants from the full 882 sample had incomplete cognitive datasets: subsequent analyses examining associations between executive function and modular segregation focused on the remaining 880 participants (Figure 1B and Figure 7).

METHOD DETAILS

Image acquisition—All MRI scans were acquired on the same 3T Siemens Tim Trio whole-body scanner and 32-channel head coil at the Hospital of the University of Pennsylvania. DTI scans were acquired using a twice- refocused spin-echo (TRSE) single-shot echo-planar imaging (EPI) sequence (TR = 8100ms, TE = 82ms, FOV = 240mm^2 / 240mm^2; Matrix = RL: 128, AP:128, Slices:70, in-plane resolution (x and y) 1.875 mm^2; slice thickness = 2mm, gap = 0; flip angle = 90°/180°/180°, volumes = 71, GRAPPA factor = 3, bandwidth = 2170 Hz/pixel, PE direction = AP). This sequence used a four-lobed diffusion encoding gradient scheme combined with a 90-180-180 spin-echo sequence designed to minimize eddy-current artifacts. For DTI acquisition, a 64-direction set was divided into two independent 32-direction imaging runs in order make scan duration more tolerable for young subjects. Each 32-direction sub-set was chosen to be maximally independent such that they separately sampled the surface of a sphere [60]. The complete sequence consisted of 64 diffusion-weighted directions with b=1000s/mm^2 and 7 interspersed scans where $b=0$ s/mm^2. The total duration of DTI scans was approximately 11 minutes. The imaging volume was prescribed in axial orientation covering the entire cerebrum with the topmost slice just superior to the apex of the brain [32]. In addition to the DTI scan, a map of the main magnetic field (i.e., B0) was derived from a double-echo, gradient-recalled echo (GRE) sequence, allowing us to estimate field distortions in each dataset.

Author Manuscript Author Manuscript Author Manuscript Author Manuscript

Image quality assurance—All DTI datasets were subject to a rigorous manual quality assessment procedure involving visual inspection of all 71 volumes [42]. Each volume was evaluated for the presence of artifact, with the total number of volumes impacted summed over the series. This scoring was based on previous work describing the impact of removing image volumes when estimating the diffusion tensor [61,62]. Data was considered "Poor" if more than 14 (20%) volumes contained artifact, "Good" if it contained 1–14 volumes with artifact, and "Excellent" if no visible artifacts were detected in any volumes. All 882 subjects included in the present study had diffusion datasets identified as "Good" or "Excellent", and had less than 2mm mean relative displacement between interspersed b=0 volumes. As described below, even after this rigorous quality assurance, motion was included as a covariate in all analyses, and the impact of motion was further evaluated in supplemental analyses.

Diffusion image preprocessing—Two consecutive 32-direction acquisitions were merged into a single 64-direction time-series. The skull was removed for each subject by registering a binary mask of a standard fractional anisotropy (FA) map (FMRIB58 FA) to each subject's DTI image using a rigid-body transformation [63]. Eddy currents and subject motion were estimated and corrected using the FSL *eddy* tool [64]. Diffusion gradient vectors were then rotated to adjust for subject motion estimated by *eddy.* After the field map was estimated, distortion correction was applied to DTI data using FSL's FUGUE [65].

Structural image processing and node definition—The structural image was processed using FreeSurfer (version 5.3) [66], and cortical and subcortical gray matter was parcellated according to the Lausanne atlas [33], which includes whole-brain sub-divisions of the Desikan-Killany anatomical atlas [67] at multiple spatial scales. Parcellations were defined in native structural space and co-registered to the first b=0 volume of each subject's diffusion image using boundary-based registration [68]. To extend gray matter region labels beyond the gray-white boundary, the atlas labels were dilated by 4mm [69]. Dilation involved filling non-labeled voxels with the statistical mode of neighboring labels. Together, 234 dilated brain regions defined the nodes for each subject's structural brain network, which was represented as a weighted adjacency matrix A.

Deterministic tractography—DTI data was imported into DSI Studio software and the diffusion tensor was estimated at each voxel [70]. For deterministic tractography, whole-brain fiber tracking was implemented for each subject in DSI Studio using a modified fiber assessment by continuous tracking (FACT) algorithm with Euler interpolation, initiating 1,000,000 streamlines after removing all streamlines with length less than 10mm or greater than 400mm. Fiber tracking was performed with an angular threshold of 45°, a step size of 0.9375mm, and a fractional anisotropy (FA) threshold determined empirically by Otzu's method, which optimizes the contrast between foreground and background [70]. FA was calculated along the path of each reconstructed streamline. For each subject, deterministic tractography served as the primary basis for constructing structural brain networks. Edges were defined where at least one streamline connected a pair of nodes end-to-end. Edge weights were primarily defined by the average FA along streamlines connecting any pair of nodes [17,30,48] (see Figure 2). In addition to these FA-weighted networks, supplemental

Author Manuscript Author Manuscript Author Manuscript Author Manuscript

analyses evaluated edge weights defined as the streamline count and streamline density using deterministic tractography (see below).

Probabilistic tractography—While deterministic tractography has high specificity relative to probabilistic methods, it suffers from a lack of sensitivity to intra-voxel fiber crossings that occur frequently throughout the brain [57,71,72]. To ensure that our results were not impacted by the failure to reconstruct crossing fibers using deterministic tractography, we fitted a ball and two-sticks diffusion model to the DTI data using the FSL *bedpostx* algorithm [72], which uses Markov chain Monte Carlo sampling to estimate the uncertainty of fiber orientations at each voxel. For probabilistic tractography, we generated subject-specific seed volumes at the FreeSurfer GM-WM boundary [39,73]. We ran FSL *probtrackx* [40], initiating 1000 probabilistic samples in each GM-WM boundary voxel identified in the 234 seed regions. A FreeSurfer segmentation of ventricles was included as an "avoidance" mask to provide anatomical constraints on tractography: all probabilistic samples entering the ventricles were discarded, and excluded from regional tractography estimates. We otherwise used default tracking parameters (a step-length of 0.5mm, 2000 steps maximum, curvature threshold of 0.02).

In order to ensure that our results were robust to different edge measures, we examined three measures of structural connectivity commonly used with probabilistic tractography. First, we constructed a symmetric N × N streamline count matrix for each subject, where edge weights were equal to the number of probabilistic streamlines connecting each pair of GM-WM boundary nodes [39,74]. Second, we constructed networks where edge weights were equal to the total number of streamlines connecting a node pair divided by their total volume [48,75,76]. Third and finally, we also constructed networks where edge weights were equal to the connectivity probability between each pair of brain regions, which represents the proportion of total samples (probabilistic streamlines) initiated from the seed region that reached the target region [77–79]. Network construction using probabilistic tractography output was implemented in MATLAB (MathWorks, Natick, MA).

While anatomical networks are classically considered sparse relative to functional networks, probabilistic tractography yields dense weighted networks that contain a large number of weak connections. The high false positive rate for probabilistic tractography often results in spurious inter-modular connections, which can have a significant detrimental impact on modularity maximization procedures, over and above the impact of false negatives [58]. Since the specificity of WM tractography methods is paramount in studies of network community structure [58], we applied a range of density thresholds to identify the strongest connections across subjects. For each of the edge-weighting schemes, probabilistic connectivity matrices were averaged across subjects, and a density threshold was applied to preserve an identical number and position of connections across subjects. Since there is no definitive choice for selecting a threshold, as in prior studies, we evaluated networks over a density range spanning 5– 60% (12 thresholds, at 5 % intervals) [73,77,80]. For example, to obtain a 5% density threshold, we retained only the 95^{th} percentile of edge weights in the group-averaged connectivity matrix. In all cases, following thresholding, edge weights in each subject's connectivity matrix were normalized by the total weight of network connections in order to delineate intrinsic topological differences across subjects

Author Manuscript Author Manuscript Author Manuscript Author Manuscript

[19,39,74,77,81–83]. For each subject, we calculated the modular segregation (mean participation coefficient) at each density threshold in order to derive integrated summary metrics [77].

Defining a priori network modules—The standard 7-system template image provided by Yeo et al. [6] was originally derived from a whole-brain clustering analysis, which yielded 7 large-scale functional networks. In order to obtain a finer-grained parcellation better suited to structural brain network construction, we calculated the *purity index* for the 7-system parcellation and brain regions from the Lausanne atlas (234- and 463-region parcellations). This measure quantifies the maximum overlap of cortical Lausanne labels and functional systems defined by Yeo et al. [6]. Each cortical Lausanne label was assigned to a functional system by calculating the non-zero mode of all voxels in each brain region. Subcortical regions were assigned to an eighth, subcortical module. The primary modular partition defined for 234-node networks is shown in Figure 2 and Figure S1.

To determine whether the functionally-defined network partition significantly fit the structural connectivity data beyond chance, we quantified the modularity quality index (formally defined below) of the functional partition imposed on structural brain networks. Briefly, the modularity quality of a network partition quantifies how well that partition maximizes the strength of within-module connections relative to a specified null model. Higher Q values indicate that modules are highly segregated within a network, with strong within-module connectivity and relatively weak between-module connectivity. We performed a permutation test to examine the significance of the modularity quality of the functional partition (Q_{Yeo}) imposed on structural connectivity matrices. First, we permuted the assignment of N nodes to functional modules 1000 times, preserving the number of nodes originally assigned to each module. We then calculated the modularity quality of randomly-defined network partitions (Q_{perm}) imposed on each subject's connectivity matrix, building a null distribution for Q_{perm}. We used the calculated mean and standard deviation of the null distribution to derive a z-score based on the observed Q_{Yeo} for each subject. Finally, we calculated the mean z-score across all subjects to assess the significance of Q_{Yeo}.

Data-driven structural network modules—Primary analyses relied on an *a priori* functional partition to define network modules, as described above. We additionally defined network modules directly from the structural connectivity data using community detection procedures. Communities were defined by maximizing the modularity quality function using a generalization of the Louvain heuristic [34,35]. Because the Louvain algorithm is degenerate [34,84], it is essential to perform modularity maximization multiple times in order to identify a stable consensus partition that accurately reflects the solutions offered by each optimization. Accordingly, we applied a Louvain-like modularity-optimization procedure [34] 100 times for each subject in order to define an "agreement" matrix A' where A'_{ij} was equal to the probability that nodes i and j were assigned to the same community over the 100 iterations. If A' was deterministic (edge weights were binary), then the algorithm had converged and the resultant partition was defined as the consensus. Otherwise, we performed 100 iterations of modularity optimization on A' in order to generate a new agreement matrix A''. This procedure was repeated until convergence [85].

Author Manuscript Author Manuscript Author Manuscript Author Manuscript

Once a consensus partition was identified for each subject, we computed a group-level consensus across the full PNC cohort (n=882). To do this, we used a Louvain-like procedure to detect communities in a group-level agreement matrix A'_{group}. Edge weights in A_{group} were equal to the proportion of times that each pair of nodes was assigned to the same community across subject-level consensus partitions. As above, 100 iterations of modularity optimization were performed on A' until the resulting A'' became binary, indicating that the algorithm had converged on a group-level consensus partition. Both subject-level and group-level consensus partitions were computed over a wide range of γ ([0, 4], in increments of 0.05) to explore variations in community structure. We plotted the number of group-level consensus modules as a function of γ, and found several plateaus indicating partition stability [86] (see Figure S2).

In order to directly compare the organization of data-driven, modularity-based partitions and the *a priori* functional partition, we quantified the partition similarity using the z-score of the Rand coefficient [87]. For two partitions X and Y, we calculated the Rand z-score in terms of the total number of node pairs in the network M, the number of pairs M_X assigned to the same module in partition X, the number of pairs M_Y that are in the same module in partition Y, and the number of pairs of nodes w_{XY} that are assigned to the same module both in partition X and in partition Y. The z-score of the Rand coefficient is defined by:

$$z_{XY} = \frac{1}{\sigma_{w_{XY}}} w_{XY} - \frac{M_X M_Y}{M}, \quad (1)$$

where σw_{XY} is the standard deviation of w_{XY}. The mean partition similarity is determined by the mean value of z_{XY} over all possible partition pairs for $X \neq Y$. Moreover, z_{XY} denotes the similarity of partitions X and Y beyond chance. Figure S2 shows the similarity between all group-level structural partitions and the primary functional partition used in this study [6].

QUANTIFICATION AND STATISTICAL ANALYSIS

Measures of modular segregation—We calculated the participation coefficient to quantify the relative balance of between-module versus within-module connectivity for each brain region [37]. Intuitively, this measure describes the degree to which a brain region integrates information across distinct modules, or the degree to which a brain region shows provincial connectivity among regions in its own module. We define the participation coefficient P_i of node i as

$$P_i = 1 - \sum_{m \in M} \left(\frac{k_i(m)}{k_i} \right)^2, \quad (2)$$

where m is a module in a set of modules M, and $k_i(m)$ is the weight of structural connections between node i and all nodes in module m [37,88]. Moreover, P_i close to 1 indicates that a brain region is highly integrated with regions in other modules, while a P_i close to 0

Author Manuscript Author Manuscript Author Manuscript Author Manuscript

indicates that a brain region is highly segregated, with strong connectivity among other regions in its own module. To quantify the segregation of specific modules, we average P_i across all brain regions assigned to the same module (see Figure 3B). To quantify global network segregation, we average P_i across all nodes in the network (see Figure 3A).

In addition to the participation coefficient, we calculated the average strength of all within-module connections (a measure of structural coherence), and the average strength of all between-module connections (a measure of structural integration) in the network [69](see Figure 4). These metrics provide additional insights into the segregation of information processing within distinct modules, and the degree to which modules are integrated across the network. While our main analyses defined partitions based on the *a priori* mapping of nodes to the modules defined by Yeo et al. [6], we also examined age effects on modular segregation (mean participation coefficient) using a data-driven structural partition defined at the group level (Figure 5B).

Alternative measures of modular segregation—As an alternative measure of modular segregation, we also calculated the modularity quality index (Q) for both group-level partitions and data-driven subject-level partitions. Q quantifies how well a given network partition maximizes the strength of within-module connections relative to a specified null model. Thus, in contrast to the participation coefficient, Q increases in more segregated brain networks. We calculated the modularity Q of a network partition S based on the following modularity quality function:

$$Q(S)=\frac{1}{2m}\sum_{ij}\left[A_{ij}-\gamma P_{ij}\right]\delta(g_i,g_j), \quad (3)$$

where m is the total weight of A, P represents the expected strength of connections according to a specified null model [1,89], γ is a structural resolution parameter that determines the size of modules, and $\delta(g_i,g_j)$ is equal to unity when brain regions i and j are assigned to same community g_i, and is zero otherwise.

We re-evaluated developmental effects when network segregation was defined by the modularity quality of the Yeo partition [6] as applied to subject-level data (Q_{Yeo} see Figure 5A). Further, we defined data-driven network partitions of each individual's structural connectivity matrix by repeating a Louvain-like modularity-optimization procedure [34,35]100 times, followed by the consensus clustering procedure described above. Consensus clustering procedures delineated subject-specific consensus partitions (defined across the optimal solutions from 100 iterations of community detection), which were used to calculate network modularity. This measure quantifies the strength of within-module connections relative to a specified null model (Q_{subj}; see Figure 5C), and was not dependent on a group-level partition.

Stability of data-driven modular partitions—To evaluate the stability of these subject-specific modular partitions across the sample age range (8–22 years), we examined whether the number of detected modules changed with age. Across partitions defined using three

Author Manuscript Author Manuscript Author Manuscript Author Manuscript

different structural resolution parameters (highlighted in Figure S2), we found no significant change in the number of detected modules with age. To examine whether the composition of group-level modular partitions evolved across development, we split our sample into three age groups corresponding to childhood (8–12 years, n=241), adolescence (13–17 years, n=451), and early adulthood (18–22 years, n=190). Group-level consensus partitions were defined for each age group using the consensus procedure described above. We evaluated consensus partitions at γ=1.5, 2.5, and 3.1, resulting in nine total partitions. Next, we calculated the partition similarity across age groups using the normalized mutual information (NMI) between each pair of partitions [46,88]. We also calculated the NMI between partitions for each age group and the data-driven consensus partitions defined across the full 882-subject sample (NMI_{Group}; see Figure S5).

Quantification of network integration—While primary analyses evaluated age-related changes in modular segregation, we were also interested in whether structural brain networks become more globally integrated during development, as previously reported [21,23]. For each subject's structural brain network represented as an adjacency matrix A, the topological length or distance of each edge A_{ij} was computed as the reciprocal of the edge weight $(\frac{1}{A_{ij}})$. The path length between any pair of nodes is defined as the sum of the edge lengths along the shortest path connecting them [88]. Global efficiency provides a theoretical prediction of how easily information can flow across a network via the shortest path between all pairs of nodes, and is defined by

$$E_{glob}(G)=\frac{1}{n}\sum_{i\in N}\frac{\sum_{j\in N,j\neq i}(d_{ij})^{-1}}{n-1}, \quad (4)$$

where n is the number of nodes, and d_{ij} is the shortest path length between node i and node j. To examine the possible role of specific edges as integrative hub connections within the network, we calculated the weighted edge betweenness centrality for each edge. Edge betweenness centrality identifies important hub connections by providing a measure of how much a given connection participates in the shortest paths of communication through a network, and thus contributes to global efficiency [45].

$$EBC=\sum_{hk}\frac{\rho_{hk}^{ij}}{\rho_{hk}}, \quad (5)$$

where ρ_{hk}^{ij} denotes the number of shortest paths between nodes h and k that include edge ij, and ρ_{hk} denotes the total number of shortest paths between h and k. After calculating edge betweenness centrality individually for each weighted network A (n=882), we normalized each subjects' edge betweenness centrality values by their maximum observed edge betweenness centrality, resulting in a bounded measure [0,1] [77]. We calculated the mean

Author Manuscript Author Manuscript Author Manuscript Author Manuscript

normalized edge betweenness centrality for each network edge across subjects, and defined *hub edges* as those connections within the top quartile of normalized edge betweenness across all network edges. Following group-level analysis, which identified a subset of edges that significantly strengthened with age, we performed a permutation-based test to assess whether connections that significantly strengthened with age were enriched for hub edges (see below).

Group-level analyses: Modular segregation—Prior work has demonstrated that brain development is not a linear process [90,91]. Accordingly, group-level analyses of structural brain network metrics were flexibly modeled using penalized splines within General Additive Models (GAM) implemented in the R package "mgcv" (https://cran.r-project.org/web/packages/mgcv/index.html) [38,92]. Such an approach allows for detection of nonlinearities in the relationship between age and measures of modular segregation without defining a set of functions *a priori* (such as polynomials). Importantly, the GAM estimates nonlinearities using restricted maximum likelihood (REML), and determines a penalty with increasing nonlinearity in order to avoid over-fitting the data. Due to this penalty, the GAM only models nonlinearities when they explain additional variance in the data above and beyond linear effects.

We used penalized splines to estimate nonlinear developmental patterns of modular segregation (Figure 3A). Within this model we included covariates for sex, head motion, and total network strength. Accordingly, the final model equations for estimating age effects on modular segregation (mean participation coefficient) were as follows:

$$\text{Modular segregation} = \text{spline(age)} + sex + \text{motion} + \text{total network strength}$$

An identical model was used when estimating age effects on the participation coefficient of individual brain regions (Figure 3C). Similarly, we applied this model across all network edges in order to assess linear and nonlinear age effects on the strength of individual connections. For all analyses, multiple comparisons were controlled using the False Discovery Rate (q<0.05) [93]. Unless otherwise specified, all statistical analyses included data from the entire sample of 882 participants.

In addition to evaluating the entire sample in one model, we also estimated age effects on modular segregation within three distinct age groups corresponding to early childhood (8–12 years, n=241), adolescence (13–17 years, n=451), and early adulthood (18–22 years, n=190) using the same model.

Group-level analyses: Network integration—To assess linear and nonlinear age effects on global network efficiency, we used the same GAM as above, controlling for the effects of sex, head motion, and total network strength (see Figure 6A). The relationship between global efficiency and modular segregation was assessed within a GAM while controlling for age in addition to other covariates described above (Figure 6B). To evaluate whether global efficiency was related to the weight of specific network connections that strengthened with age, we assessed the relationship between global efficiency and the average strength of within-module edges (Figure 6E), or the relationship between global

Author Manuscript Author Manuscript Author Manuscript Author Manuscript

efficiency and the average strength of between-module edges (Figure 6F), while controlling for age and the same covariates described above.

Associations with executive function—We assessed linear and nonlinear age effects on executive function by modeling a spline age term within a GAM while controlling for sex (Figure 1B). To examine the association between modular segregation and executive efficiency, we included a spline age term in the model to account for the variance associated with linear and nonlinear age-related changes in executive ability. The final model equation was as follows:

$$\text{Modular segregation} = \text{spline(age)} + \text{executive efficiency} + sex + \text{motion} + \text{total network strength}$$

We also evaluated the association between the segregation of individual modules (e.g., frontoparietal) and three cognitive efficiency factor scores: executive function, memory, and social cognition (see Figure 7A). Two participants from the full 882 sample had incomplete cognitive datasets; thus associations with cognition were evaluated in the remaining 880 participants.

Mediation analyses—Linear mediation analyses investigated whether age-related improvement in executive function was mediated by modular segregation and/or global efficiency [94]. First, we regressed out the effects of nuisance covariates (sex, head motion, and total network strength) on the independent (X), dependent (Y), and mediating (M) variables. The residuals were then used in our mediation analysis. The significance of the indirect effect was evaluated using bootstrapped confidence intervals within the R package "lavaan" (https://cran.r-project.org/web/packages/lavaan/).

Specifically, we examined the total effect of age on executive performance (c path; Figure 7B), the relationship between age and modular segregation (a path), the relationship between modular segregation and executive function (b path), and the direct effect of age on executive efficiency after including modular segregation as a mediator in the model (c' path). The significance of the indirect effect of age on executive function through the proposed mediator (modular segregation) was tested using bootstrapping procedures, which minimize assumptions about the sampling distribution [94]. This approach involves calculating unstandardized indirect effects for each of 10,000 bootstrapped samples and calculating the 95% confidence interval. This procedure was repeated to assess both other domains of cognition (memory, social cognition) as well as the specific mediating effects of each network module (e.g., the frontoparietal module). Finally, we evaluated whether age-related increases in global efficiency also mediated improvements in executive function.

Edge-based permutation testing—We performed permutation-based tests across network edges in order to assess (*i*) whether the edges that significantly strengthened with age were localized to within-module connections beyond chance, (*ii*) whether edges that significantly strengthen with age were enriched for hub edges, and (*iii*) whether these edges that strengthen with age had elevated edge betweenness centrality beyond chance.

Author Manuscript Author Manuscript Author Manuscript Author Manuscript

First, we permuted a binary edge label specifying whether each edge connects nodes within or between modules 1000 times. Then for permuted samples of within- and between-module edges, we counted the number of edges that were shown to significantly strengthen with age in group-level analysis. We then rank-ordered the number of edges shown to significantly strengthen with age for permuted within-module edge samples, and determined where the observed number of within-module edges that strengthen with age falls relative to this null distribution (see Figure 4D).

Second, we evaluated whether edges that significantly strengthen with age were enriched for hub edges. We permuted a binary edge label defining hub or non-hub edges 1000 times. For each permuted sample, we counted the number of edges that significantly strengthened with age in group-level analysis. Then, we rank-ordered the number of permuted hub edges shown to significantly strengthen with age, and compared these values with the observed number of hub edges that strengthened with age.

Third, we evaluated whether edges that significantly strengthen with age had higher edge betweenness centrality than anticipated by chance. We permuted normalized edge betweenness centrality values 1000 times. For each permuted sample, we calculated the mean edge betweenness centrality of within-module edges and between-module edges that significantly strengthened with age. We rank-ordered the mean edge betweenness centrality of permuted within-module and between- module edges that strengthened with age, and separately compared these values with the observed mean of within- and between-module edges (see Figure 6D).

Overview of sensitivity analyses—We conducted a thorough set of analyses to examine whether our results were dependent on specific analytic choices. These included alternative node and edge definitions, use of probabilistic instead of deterministic tractography, and alternative network normalization. Furthermore, we conducted sensitivity analyses to examine the potential impact of short-range connections, and un-modeled subject variables.

Alternative node and edge definitions—In order to evaluate whether our results were dependent on a specific aspects of network definition, we examined alternative node and edge definitions. First, we examined modular segregation (mean participation coefficient) using the *a priori* functional partition assigned to a higher-resolution parcellation of the brain from the Lausanne atlas (463 nodes instead of 234; see Figure 5D).

Next, we examined alternative edge weight definitions. While primary analyses focused on FA-weighted structural networks, we also measured modular segregation in streamline-weighted networks (see Figure 5E), where edge weights were equal to the number of streamlines connecting a pair of nodes [19]. Additionally, we measured modular segregation in streamline density-weighted networks, where edge weights were defined as the number of connecting streamlines divided by the total regional volume of each node pair [48] (see Figure 5F).

Author Manuscript Author Manuscript Author Manuscript Author Manuscript

Alternative tractography method—We also assessed developmental effects on modular segregation using brain networks constructed with probabilistic tractography (see above). Mean participation coefficients were calculated for each subject's connectivity matrix and integrated across the 12 density thresholds to derive a summary metric of modular segregation [77]. Integrated participation coefficients were calculated for networks with three different edge weight definitions: probabilistic streamline count, probabilistic streamline density, and inter-regional connectivity probability (see Figure 5G–I).

Alternative network normalization—Network normalization is imperative when evaluating between-subject differences in network topology [39,77,81], as global effects may mask intrinsic topological differences. Normalization can be applied at either the subject-level or group-level [81,82]. Subject-level normalization has been widely applied in brain network studies using probabilistic tractography, and involves dividing each unique element of the weighted connectivity matrix by the sum of all connection weights [74,77,82,83]. Based on the work of Yan et al. [81], which suggests that subject-level normalization may introduce artifactual relationships with response variables, we applied a group-level normalization by including total network strength as a covariate in GAMs. To ensure that results were robust to an alternative subject-level normalization procedure, we recalculated network measures after dividing elements of each subject's FA-weighted connectivity matrix by the total network strength. We then estimated age effects on normalized topological measures using a GAM, including sex and in-scanner motion as covariates as above.

Assessment of short-range connections—Estimates of short-range connectivity are often inflated due to the well-documented distance-related bias in diffusion tractography methods [95]. To determine the extent to which age effects on modular segregation were driven by the (potentially artifactual) strengthening of short-range connections, we applied Euclidean distance-based thresholds to subject connectivity matrices, removing all connections less than 20mm, 25mm, and 30mm [5,96]. We then recalculated measures of modular segregation (mean participation coefficient) for each subject and estimated age effects at the group level (see Figure S6).

Potentially confounding subject variables—Brain developmental processes are extremely complex, with multiple factors potentially influencing network-level measures of brain maturation [97]. Accordingly, as a final step, we evaluated whether results could be explained by un-modeled covariates which could potentially confound inference. First, to ensure that the observed age-related increase in modular segregation was not driven by global changes in white matter volume or anisotropy, we included these measures as additional covariates in the GAM described above. Second, we evaluated whether other subject-level covariates could explain the observed developmental effects. We also found convergent results when including total brain volume, handedness, race, and maternal education as covariates in GAMs estimating age effects on modular segregation. Conversely, results remained consistent when all covariates were removed from the model. Third and finally, in order to ensure that our results were not driven by age-related differences in head motion, we conducted a sensitivity analysis in a sub-sample of subjects who had low head

Author Manuscript Author Manuscript Author Manuscript Author Manuscript

motion (less than 0.5mm mean frame-wise displacement). In this subset of 619 subjects, there was no longer a significant correlation between age and motion, or between modular segregation and motion. See Figure S7.

DATA AND SOFTWARE AVAILABILITY

The data reported in this paper have been deposited in the database of Genotypes and Phenotypes (https://www.ncbi.nlm.nih.gov/proiects/gap/cgi-bin/study_cgi?study_id=phs000607.v1.p1). Table S2 details publicly-available MATLAB code used to calculate brain network measures.

TABLE FOR AUTHOR TO COMPLETE

Please upload the completed table as a separate document. **Please do not add subheadings to the Key Resources Table.** If you wish to make an entry that does not fall into one of the subheadings below, please contact your handling editor.

Supplementary Material

Refer to Web version on PubMed Central for supplementary material.

Acknowledgments

We thank the acquisition and recruitment team, including Karthik Prabhakaran and Jeff Valdez. Thanks to Chad Jackson for data management and systems support and Monica Calkins for phenotyping expertise. Supported by grants from the National Institute of Mental Health: R01MH107703 (TDS), R21MH106799 (DSB & TDS). DSB acknowledges support from the John D. and Catherine T. MacArthur Foundation, the Alfred P. Sloan Foundation, the Army Research Laboratory and the Army Research Office through contract numbers W911NF-10-2-0022 and W911NF-14-1-0679, the National Institute of Mental Health (R01-DC-009209-11), the National Institute of Child Health and Human Development (R01HD086888-01), the Office of Naval Research, and the National Science Foundation (BCS-1441502, BCS-1430087, and PHY-1554488). The PNC was funded through NIMH RC2 grants MH089983 and MH089924 (REG). Additional support was provided by R01MH107235 (RCG), K01MH102609 (DRR), P50MH096891 (REG), R01NS085211 (RTS), and the Dowshen Program for Neuroscience. Support for developing statistical analyses (RTS & TDS) was provided by a seed grant by the Center for Biomedical Computing and Image Analysis (CBICA) at Penn.

References

1. Newman MEJ. Modularity and community structure in networks. Proc Natl Acad Sci USA. 2006; 103:8577–82. [PubMed: 16723398]
2. Sporns O, Betzel RF. Modular Brain Networks. Annu Rev Psychol. 2016; 67:613–640. [PubMed: 26393868]
3. Biswal B, Yetkin FZ, Haughton VM, Hyde JS. Functional connectivity in the motor cortex of resting human brain using echo-planar MRI. Magn Reson Med. 1995; 34:537–41. [PubMed: 8524021]
4. Damoiseaux JS, Rombouts S, Barkhof F, Scheltens P, Stam CJ, Smith SM, Beckmann CF. Consistent resting-state networks across healthy subjects. Proc Natl Acad Sci USA. 2006; 103:13848–13853. [PubMed: 16945915]
5. Power JD, Cohen AL, Nelson SM, Wig GS, Barnes KA, Church JA, Vogel AC, Laumann TO, Miezin FM, Schlaggar BL, et al. Functional network organization of the human brain. Neuron. 2011; 72:665–78. [PubMed: 22099467]
6. Yeo BTT, Krienen FM, Sepulcre J, Sabuncu MR, Lashkari D, Hollinshead M, Roffman JL, Smoller JW, Zöllei L, Polimeni JR, et al. The organization of the human cerebral cortex estimated by intrinsic functional connectivity. J Neurophysiol. 2011; 106:1125–1165. [PubMed: 21653723]

Author Manuscript Author Manuscript Author Manuscript Author Manuscript

7. van den Heuvel MP, Kersbergen KJ, de Reus MA, Keunen K, Kahn RS, Groenendaal F, de Vries LS, Benders MJNL. The Neonatal Connectome During Preterm Brain Development. Cereb Cortex. 2015; 25:3000–13. [PubMed: 24833018]
8. Fair DA, Cohen AL, Power JD, Dosenbach NUF, Church JA, Miezin FM, Schlaggar BL, Petersen SE. Functional brain networks develop from a “local to distributed” organization. PLoS Comput Biol. 2009; 5:e1000381. [PubMed: 19412534]
9. Gu S, Satterthwaite TD, Medaglia JD, Yang M, Gur RE, Gur RC, Bassett DS. Emergence of system roles in normative neurodevelopment. Proc Natl Acad Sci USA. 2015; 112:13681–13686. [PubMed: 26483477]
10. Dosenbach NUF, Nardos B, Cohen AL, Fair DA, Power JD, Church JA, Nelson SM, Wig GS, Vogel AC, Lessov-Schlaggar CN, et al. Prediction of individual brain maturity using fMRI. Science. 2010; 329:1358–61. [PubMed: 20829489]
11. Satterthwaite TD, Wolf DH, Ruparel K, Erus G, Elliott MA, Eickhoff SB, Gennatas ED, Jackson C, Prabhakaran K, Smith A, et al. Heterogeneous impact of motion on fundamental patterns of developmental changes in functional connectivity during youth. NeuroImage. 2013; 83:45–57.
12. Hampson M, Driesen N, Roth JK, Gore JC, Constable RT. Functional connectivity between task-positive and task-negative brain areas and its relation to working memory performance. Magn Reson Imaging. 2010; 28:1051–7. [PubMed: 20409665]
13. Satterthwaite TD, Wolf DH, Erus G, Ruparel K, Elliott MA, Gennatas ED, Hopson R, Jackson C, Prabhakaran K, Bilker WB, et al. Functional Maturation of the Executive System during Adolescence. J Neurosci. 2013; 33:16249–16261. [PubMed: 24107956]
14. Betzel RF, Byrge L, He Y, Goñi J, Zuo XNN, Sporns O. Changes in structural and functional connectivity among resting-state networks across the human lifespan. NeuroImage. 2014; 102(Pt 2):345–357. [PubMed: 25109530]
15. Honey CJ, Sporns O, Cammoun L, Gigandet X, Thiran JP, Meuli R, Hagmann P. Predicting human resting-state functional connectivity from structural connectivity. Proc Natl Acad Sci USA. 2009; 106:2035–2040. [PubMed: 19188601]
16. Goñi J, van den Heuvel MP, Avena-Koenigsberger A, de Mendizabal N, Betzel RF, Griffa A, Hagmann P, Corominas-Murtra B, Thiran JPP, Sporns O. Resting-brain functional connectivity predicted by analytic measures of network communication. Proc Natl Acad Sci USA. 2014; 111:833–838. [PubMed: 24379387]
17. Mišić B, Betzel RF, de Reus MA, van den Heuvel MP, Berman MG, McIntosh AR, Sporns O. Network-Level Structure-Function Relationships in Human Neocortex. Cereb Cortex. 2016; 26:3285–3296. [PubMed: 27102654]
18. Hermundstad AM, Bassett DS, Brown KS, Aminoff EM, Clewett D, Freeman S, Frithsen A, Johnson A, Tipper CM, Miller MB, et al. Structural foundations of resting-state and task-based functional connectivity in the human brain. Proc Natl Acad Sci USA. 2013; 110:6169–6174. [PubMed: 23530246]
19. Bassett DS, Brown JA, Deshpande V, Carlson JM, Grafton ST. Conserved and variable architecture of human white matter connectivity. NeuroImage. 2011; 54:1262–1279. [PubMed: 20850551]
20. Bassett DS, Greenfield DL, Meyer-Lindenberg A, Weinberger DR, Moore SW, Bullmore ET. Efficient physical embedding of topologically complex information processing networks in brains and computer circuits. PLoS Comput Biol. 2010; 6:e1000748. [PubMed: 20421990]
21. Chen Z, Liu M, Gross DW, Beaulieu C. Graph theoretical analysis of developmental patterns of the white matter network. Front Hum Neurosci. 2013; 7:716. [PubMed: 24198774]
22. Huang H, Shu N, Mishra V, Jeon T, Chalak L, Wang ZJ, Rollins N, Gong G, Cheng H, Peng Y, et al. Development of human brain structural networks through infancy and childhood. Cereb Cortex. 2015; 25:1389–404. [PubMed: 24335033]
23. Hagmann P, Sporns O, Madan N, Cammoun L, Pienaar R, Wedeen VJ, Meuli R, Thiran JPP, Grant PE. White matter maturation reshapes structural connectivity in the late developing human brain. Proc Natl Acad Sci USA. 2010; 107:19067–19072. [PubMed: 20956328]
24. Lim S, Han CE, Uhlhaas PJ, Kaiser M. Preferential detachment during human brain development: age- and sex-specific structural connectivity in diffusion tensor imaging (DTI) data. Cereb Cortex. 2015; 25:1477–89. [PubMed: 24343892]

Author Manuscript Author Manuscript Author Manuscript Author Manuscript

25. Gur RC, Richard J, Calkins ME, Chiavacci R, Hansen JA, Bilker WB, Loughead J, Connolly JJ, Qiu H, Mentch FD, et al. Age group and sex differences in performance on a computerized neurocognitive battery in children age 8–21. Neuropsychology. 2012; 26:251–65. [PubMed: 22251308]
26. Casey BJ, Jones RM, Hare TA. The Adolescent Brain. Ann N Y Acad Sci. 2008; 1124:111–126. [PubMed: 18400927]
27. Insel TR. Rethinking schizophrenia. Nature. 2010; 468:187–193. [PubMed: 21068826]
28. Shanmugan S, Wolf DH, Calkins ME, Moore TM, Ruparel K, Hopson RD, Vandekar SN, Roalf DR, Elliott MA, Jackson C, et al. Common and Dissociable Mechanisms of Executive System Dysfunction Across Psychiatric Disorders in Youth. Am J Psychiatry. 2016; 173:517–526. [PubMed: 26806874]
29. Di Martino A, Fair DA, Kelly C, Satterthwaite TD, Castellanos FX, Thomason ME, Craddock RC, Luna B, Leventhal BL, Zuo XNN, et al. Unraveling the miswired connectome: a developmental perspective. Neuron. 2014; 83:1335–1353. [PubMed: 25233316]
30. Bohlken MM, Brouwer RM, Mandl RCW, den Heuvel MP, Hedman AM, De Hert M, Cahn W, Kahn RS, Hulshoff Pol HE. Structural Brain Connectivity as a Genetic Marker for Schizophrenia. JAMA Psychiatry. 2016; 73:11–19. [PubMed: 26606729]
31. Kessler D, Angstadt M, Sripada C. Growth Charting of Brain Connectivity Networks and the Identification of Attention Impairment in Youth. JAMA Psychiatry. 2016; 73:481–489. [PubMed: 27076193]
32. Satterthwaite TD, Elliott MA, Ruparel K, Loughead J, Prabhakaran K, Calkins ME, Hopson R, Jackson C, Keefe J, Riley M. Neuroimaging of the Philadelphia neurodevelopmental cohort. NeuroImage. 2014; 86:544–553. [PubMed: 23921101]
33. Cammoun L, Gigandet X, Meskaldji D, Thiran JP, Sporns O, Do KQ, Maeder P, Meuli R, Hagmann P. Mapping the human connectome at multiple scales with diffusion spectrum MRI. J Neurosci Methods. 2012; 203:386–397. [PubMed: 22001222]
34. Blondel VD, Guillaume JLL, Lambiotte R, Lefebvre E. Fast unfolding of communities in large networks. J Stat Mech Theory Exp. 2008; 2008:P10008.
35. Mucha PJ, Richardson T, Macon K, Porter MA, Onnela JPP. Community structure in time-dependent, multiscale, and multiplex networks. Science. 2010; 328:876–878. [PubMed: 20466926]
36. Bassett DS, Porter MA, Wymbs NF, Grafton ST, Carlson JM, Mucha PJ. Robust detection of dynamic community structure in networks. Chaos. 2013; 23:13142.
37. Guimerà R, Amaral LAN. Cartography of complex networks: modules and universal roles. J Stat Mech. 2005; 2005:nihpa35573. [PubMed: 18159217]
38. Wood SN. Stable and efficient multiple smoothing parameter estimation for generalized additive models. J Am Stat Assoc. 2012
39. Li L, Rilling JK, Preuss TM, Glasser MF, Hu X. The effects of connection reconstruction method on the interregional connectivity of brain networks via diffusion tractography. Hum Brain Mapp. 2012; 33:1894–1913. [PubMed: 21928316]
40. Behrens TEJ, Berg HJ, Jbabdi S, Rushworth MFS, Woolrich MW. Probabilistic diffusion tractography with multiple fibre orientations: What can we gain? NeuroImage. 2007; 34:144–155. [PubMed: 17070705]
41. Yendiki A, Koldewyn K, Kakunoori S, Kanwisher N, Fischl B. Spurious group differences due to head motion in a diffusion MRI study. Neuroimage. 2014; 88:79–90. [PubMed: 24269273]
42. Roalf DR, Quarmley M, Elliott MA, Satterthwaite TD, Vandekar SN, Ruparel K, Gennatas ED, Calkins ME, Moore TM, Hopson R. The impact of quality assurance assessment on diffusion tensor imaging outcomes in a large-scale population-based cohort. NeuroImage. 2016; 125:903–919. [PubMed: 26520775]
43. Latora V, Marchiori M. Efficient behavior of small-world networks. Phys Rev Lett. 2001; 87:198701. [PubMed: 11690461]
44. Bertolero MA, Yeo BTT, D'Esposito M. The modular and integrative functional architecture of the human brain. Proc Natl Acad Sci USA. 2015; 112:E6798–807. [PubMed: 26598686]
45. Brandes U. A faster algorithm for betweenness centrality. J Math Sociol. 2001; 25:163–177.

Author Manuscript Author Manuscript Author Manuscript Author Manuscript

46. Marek S, Hwang K, Foran W, Hallquist MN, Luna B. The Contribution of Network Organization and Integration to the Development of Cognitive Control. PLoS Biol. 2015; 13:e1002328. [PubMed: 26713863]
47. Zalesky A, Fornito A, Harding IH, Cocchi L, Yücel M, Pantelis C, Bullmore ET. Whole-brain anatomical networks: does the choice of nodes matter? NeuroImage. 2010; 50:970–983. [PubMed: 20035887]
48. Baker STE, Lubman DI, Yücel M, Allen NB, Whittle S, Fulcher BD, Zalesky A, Fornito A. Developmental Changes in Brain Network Hub Connectivity in Late Adolescence. J Neurosci. 2015; 35:9078–9087. [PubMed: 26085632]
49. Buckner RL, Andrews-Hanna JR, Schacter DL. The brain's default network: anatomy, function, and relevance to disease. Ann N Acad Sci. 2008; 1124:1–38.
50. Fornito A, Harrison BJ, Zalesky A, Simons JS. Competitive and cooperative dynamics of large-scale brain functional networks supporting recollection. Proc Natl Acad Sci USA. 2012; 109:12788–93. [PubMed: 22807481]
51. Braun U, Schäfer A, Walter H, Erk S, Romanczuk-Seiferth N, Haddad L, Schweiger JI, Grimm O, Heinz A, Tost H, et al. Dynamic reconfiguration of frontal brain networks during executive cognition in humans. Proc Natl Acad Sci USA. 2015; 112:11678–11683. [PubMed: 26324898]
52. Mohr H, Wolfensteller U, Betzel RF, Mišić B, Sporns O, Richiardi J, Ruge H. Integration and segregation of large-scale brain networks during short-term task automatization. Nat Commun. 2016; 7:13217. [PubMed: 27808095]
53. Kraemer HC, Yesavage JA, Taylor JL, Kupfer D. How can we learn about developmental processes from cross-sectional studies, or can we? Am J Psychiatry. 2000; 157:163–171. [PubMed: 10671382]
54. Schumann G, Loth E, Banaschewski T, Barbot A, Barker G, Büchel C, Conrod PJ, Dalley JW, Flor H, Gallinat J, et al. The IMAGEN study: reinforcement-related behaviour in normal brain function and psychopathology. Mol Psychiatry. 2010; 15:1128–39. [PubMed: 21102431]
55. Nooner KB, Colcombe SJ, Tobe RH, Mennes M, Benedict MM, Moreno AL, Panek LJ, Brown S, Zavitz ST, Li Q, et al. The NKI-Rockland Sample: A Model for Accelerating the Pace of Discovery Science in Psychiatry. Front Neurosci. 2012; 6:152. [PubMed: 23087608]
56. Jbabdi S, Sotiropoulos SN, Haber SN, Van Essen DC, Behrens TE. Measuring macroscopic brain connections in vivo. Nat Neurosci. 2015; 18:1546–1555. [PubMed: 26505566]
57. Thomas C, Ye FQ, Irfanoglu MO, Modi P, Saleem KS, Leopold DA, Pierpaoli C. Anatomical accuracy of brain connections derived from diffusion MRI tractography is inherently limited. Proc Natl Acad Sci USA. 2014; 111:16574–16579. [PubMed: 25368179]
58. Zalesky A, Fornito A, Cocchi L, Gollo LL, van den Heuvel MP, Breakspear M. Connectome sensitivity or specificity: which is more important? NeuroImage. 2016; 142:407–420. [PubMed: 27364472]
59. Moore TM, Reise SP, Gur RE, Hakonarson H, Gur RC. Psychometric Properties of the Penn Computerized Neurocognitive Battery. Neuropsychology. 2014
60. Jones DK, Griffin LD, Alexander DC, Catani M, Horsfield MA, Howard R, Williams SCR. Spatial normalization and averaging of diffusion tensor MRI data sets. NeuroImage. 2002; 17:592–617. [PubMed: 12377137]
61. Chen Y, Tymofiyeva O, Hess CP, Xu D. Effects of rejecting diffusion directions on tensor-derived parameters. NeuroImage. 2015; 109:160–170. [PubMed: 25585018]
62. Jones DK, Basser PJ. Squashing peanuts and smashing pumpkins": How noise distorts diffusion-weighted MR data. Magn Reson Med. 2004; 52:979–993. [PubMed: 15508154]
63. Jenkinson M, Bannister P, Brady M, Smith S. Improved optimization for the robust and accurate linear registration and motion correction of brain images. NeuroImage. 2002; 17:825–841. [PubMed: 12377157]
64. Andersson JLR, Sotiropoulos SN. An integrated approach to correction for off-resonance effects and subject movement in diffusion MR imaging. NeuroImage. 2016; 125:1063–78. [PubMed: 26481672]
65. Jenkinson M, Beckmann CF, Behrens TE, Woolrich MW, Smith SM. Fsl. Neuroimage. 2012; 62:782–790. [PubMed: 21979382]

Author Manuscript Author Manuscript Author Manuscript Author Manuscript

66. Fischl B. FreeSurfer. NeuroImage. 2012; 62:774–781. [PubMed: 22248573]
67. Desikan RS, Ségonne F, Fischl B, Quinn BT, Dickerson BC, Blacker D, Buckner RL, Dale AM, Maguire RP, Hyman BT, et al. An automated labeling system for subdividing the human cerebral cortex on MRI scans into gyral based regions of interest. NeuroImage. 2006; 31:968–980. [PubMed: 16530430]
68. Greve DN, Fischl B. Accurate and robust brain image alignment using boundary-based registration. NeuroImage. 2009; 48:63–72. [PubMed: 19573611]
69. Gu S, Pasqualetti F, Cieslak M, Telesford QK, Yu AB, Kahn AE, Medaglia JD, Vettel JM, Miller MB, Grafton ST, et al. Controllability of structural brain networks. Nat Commun. 2015; 6:8414. [PubMed: 26423222]
70. Yeh FC, Verstynen TD, Wang Y, Fernández-Miranda JC, Tseng WYI. Deterministic Diffusion Fiber Tracking Improved by Quantitative Anisotropy. PLoS ONE. 2013; 8:e80713. [PubMed: 24348913]
71. Jeurissen B, Leemans A, Tournier JDD, Jones DK, Sijbers J. Investigating the prevalence of complex fiber configurations in white matter tissue with diffusion magnetic resonance imaging. Hum Brain Mapp. 2013; 34:2747–66. [PubMed: 22611035]
72. Behrens TEJ, Woolrich MW, Jenkinson M, Johansen-Berg H, Nunes RG, Clare S, Matthews PM, Brady JM, Smith SM. Characterization and propagation of uncertainty in diffusion-weighted MR imaging. Magn Reson Med. 2003; 50:1077–88. [PubMed: 14587019]
73. Li L, Hu X, Preuss TM, Glasser MF, Damen FW, Qui Y, Rilling J. Mapping putative hubs in human, chimpanzee and rhesus macaque connectomes via diffusion tractography. NeuroImage. 2013; 80:462–74. [PubMed: 23603286]
74. Duarte-Carvajalino JM, Jahanshad N, Lenglet C, McMahon KL, de Zubicaray GI, Martin NG, Wright MJ, Thompson PM, Sapiro G. Hierarchical topological network analysis of anatomical human brain connectivity and differences related to sex and kinship. Neuroimage. 2012; 59:3784–804. [PubMed: 22108644]
75. van den Heuvel MP, Sporns O. Rich-club organization of the human connectome. J Neurosci. 2011; 31:15775–86. [PubMed: 22049421]
76. van den Heuvel MP, de Reus MA, Feldman Barrett L, Scholtens LH, Coopmans FMT, Schmidt R, Preuss TM, Rilling JK, Li L. Comparison of diffusion tractography and tract-tracing measures of connectivity strength in rhesus macaque connectome. Hum Brain Mapp. 2015; 36:3064–75. [PubMed: 26058702]
77. Gong G, Rosa-Neto P, Carbonell F, Chen ZJ, He Y, Evans AC. Age- and gender-related differences in the cortical anatomical network. J Neurosci. 2009; 29:15684–93. [PubMed: 20016083]
78. Johansen-Berg H, Behrens TEJ, Sillery E, Ciccarelli O, Thompson AJ, Smith SM, Matthews PM. Functional-anatomical validation and individual variation of diffusion tractography-based segmentation of the human thalamus. Cereb Cortex. 2005; 15:31–9. [PubMed: 15238447]
79. Cao Q, Shu N, An L, Wang P, Sun L, Xia MRR, Wang JHH, Gong GLL, Zang YFF, Wang YFF, et al. Probabilistic diffusion tractography and graph theory analysis reveal abnormal white matter structural connectivity networks in drug-naive boys with attention deficit/hyperactivity disorder. J Neurosci. 2013; 33:10676–87. [PubMed: 23804091]
80. Achard S, Bullmore E. Efficiency and cost of economical brain functional networks. PLoS Comput Biol. 2007; 3:e17. [PubMed: 17274684]
81. Yan CGG, Craddock RC, Zuo XNN, Zang YFF, Milham MP. Standardizing the intrinsic brain: towards robust measurement of inter-individual variation in 1000 functional connectomes. NeuroImage. 2013; 80:246–62. [PubMed: 23631983]
82. Zhan L, Zhou J, Wang Y, Jin Y, Jahanshad N, Prasad G, Nir TM, Leonardo CD, Ye J, Thompson PM, et al. Comparison of nine tractography algorithms for detecting abnormal structural brain networks in Alzheimer's disease. Front Aging Neurosci. 2015; 7:48. [PubMed: 25926791]
83. Dennis EL, Jahanshad N, McMahon KL, de Zubicaray GI, Martin NG, Hickie IB, Toga AW, Wright MJ, Thompson PM. Development of brain structural connectivity between ages 12 and 30: a 4-Tesla diffusion imaging study in 439 adolescents and adults. NeuroImage. 2013; 64:671–84. [PubMed: 22982357]

Author Manuscript Author Manuscript Author Manuscript Author Manuscript

84. Good BH, de Montjoye YAA, Clauset A. Performance of modularity maximization in practical contexts. Phys Rev E Stat Nonlin Soft Matter Phys. 2010; 81:46106.

85. Lancichinetti A, Fortunato S. Consensus clustering in complex networks. Sci Rep. 2012; 2:336. [PubMed: 22468223]

86. Fenn DJ, Porter MA, McDonald M, Williams S, Johnson NF, Jones NS. Dynamic communities in multichannel data: an application to the foreign exchange market during the 2007–2008 credit crisis. Chaos. 2009; 19:33119.

87. Traud A, Kelsic E, Mucha P, Porter M. Comparing Community Structure to Characteristics in Online Collegiate Social Networks. SIAM Rev. 2011; 53:526–543.

88. Rubinov M, Sporns O. Complex network measures of brain connectivity: uses and interpretations. NeuroImage. 2010; 52:1059–1069. [PubMed: 19819337]

89. Newman MEJ, Girvan M. Finding and evaluating community structure in networks. Phys Rev E Stat Nonlin Soft Matter Phys. 2004; 69:26113.

90. Gogtay N, Giedd JN, Lusk L, Hayashi KM, Greenstein D, Vaituzis AC, Nugent TF, Herman DH, Clasen LS, Toga AW, et al. Dynamic mapping of human cortical development during childhood through early adulthood. Proc Natl Acad Sci USA. 2004; 101:8174–9. [PubMed: 15148381]

91. Shaw P, Greenstein D, Lerch J, Clasen L, Lenroot R, Gogtay N, Evans A, Rapoport J, Giedd J. Intellectual ability and cortical development in children and adolescents. Nature. 2006; 440:676–679. [PubMed: 16572172]

92. Wood SN. Fast stable restricted maximum likelihood and marginal likelihood estimation of semiparametric generalized linear models. J R Stat Soc Ser B Stat Methodol. 2011; 73:3–36.

93. Genovese CR, Lazar NA, Nichols T. Thresholding of statistical maps in functional neuroimaging using the false discovery rate. NeuroImage. 2002; 15:870–8. [PubMed: 11906227]

94. Preacher KJ, Hayes AF. Asymptotic and resampling strategies for assessing and comparing indirect effects in multiple mediator models. Behav Res Methods. 2008; 40:879–91. [PubMed: 18697684]

95. Girard G, Whittingstall K, Deriche R, Descoteaux M. Towards quantitative connectivity analysis: reducing tractography biases. NeuroImage. 2014; 98:266–78. [PubMed: 24816531]

96. Power JD, Schlaggar BL, Lessov-Schlaggar CN, Petersen SE. Evidence for hubs in human functional brain networks. Neuron. 2013; 79:798–813. [PubMed: 23972601]

97. Hagmann P, Grant PE, Fair DA. MR connectomics: a conceptual framework for studying the developing brain. Front Syst Neurosci. 2012; 6:43. [PubMed: 22707934]

Author Manuscript Author Manuscript Author Manuscript Author Manuscript

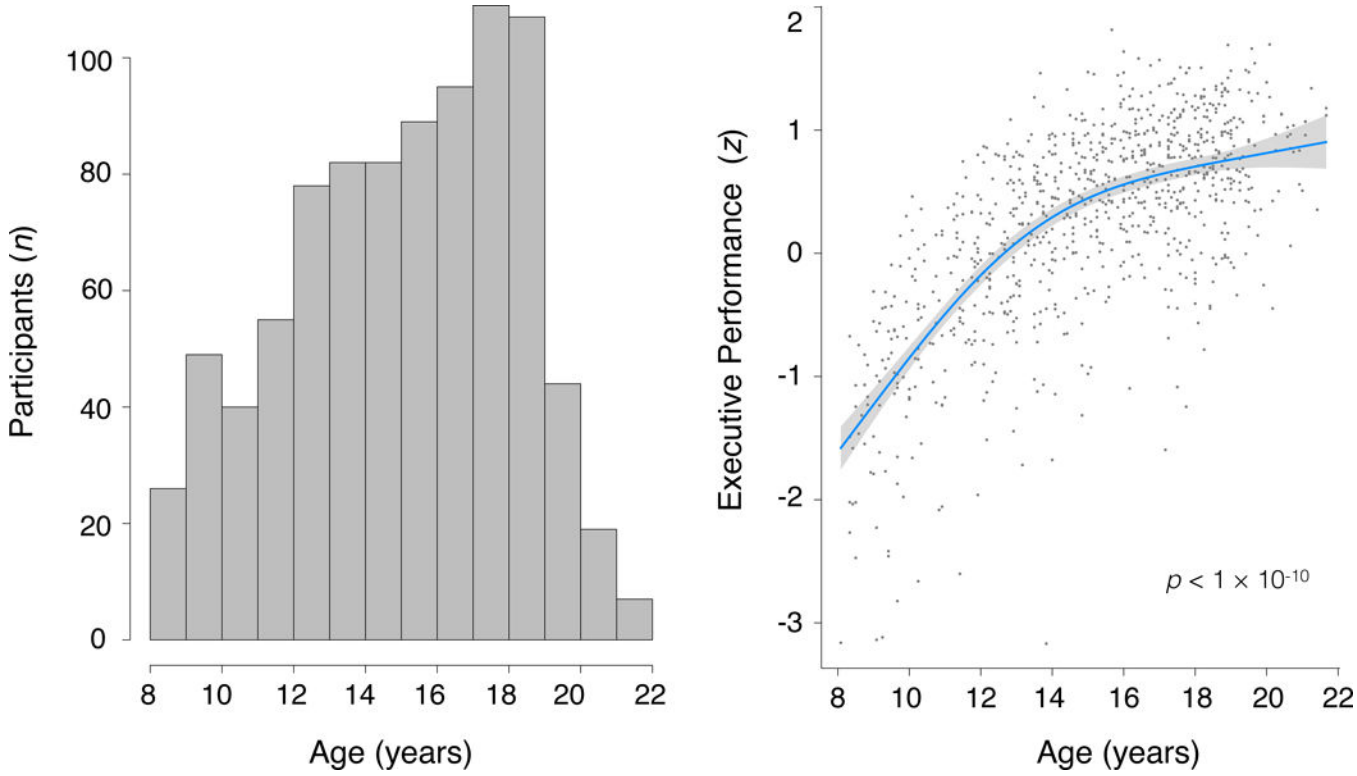

Figure 1. Executive functioning improves with age

(**A**) Age distribution of 882 youth completing diffusion imaging as part of the PNC. (**B**) Executive performance on a neurocognitive battery improves with age (n=880). Blue line represents the best fit from a general additive model; shaded area indicates 95% confidence interval.

Author Manuscript Author Manuscript Author Manuscript Author Manuscript

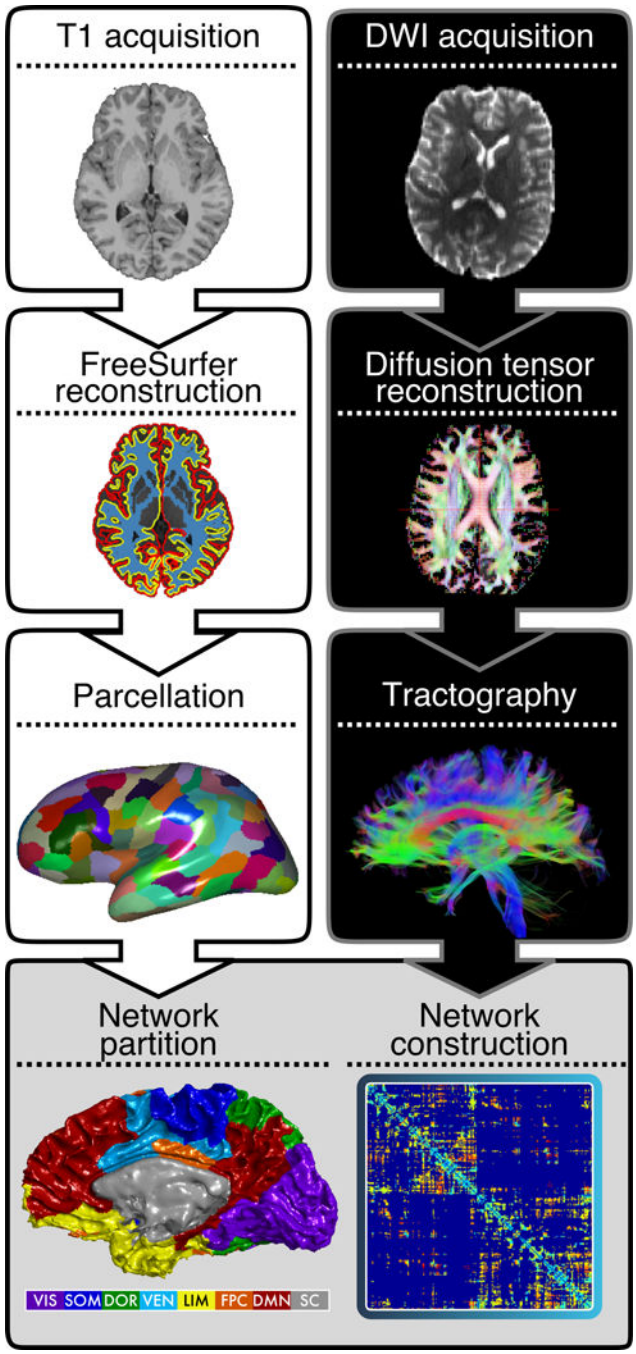

Figure 2. Connectome construction

For each subject, the T1 image was processed using FreeSurfer and parcellated into 234 network nodes on an individualized basis. Deterministic streamline tractography was used to create a symmetric adjacency matrix (234×234), where the edge weight was defined as the mean fractional anisotropy (FA) along the connecting streamlines. Network nodes were each assigned to one of the seven large-scale functional modules defined by Yeo et al. [6]; subcortical nodes were assigned to an eighth module. VIS=visual, SOM=somatomotor,

DOR=dorsal attention, VEN=ventral attention, LIM=limbic, FPC=frontoparietal control, DMN= default mode network, SUB=subcortical.

Author Manuscript Author Manuscript Author Manuscript Author Manuscript

Author Manuscript Author Manuscript Author Manuscript Author Manuscript

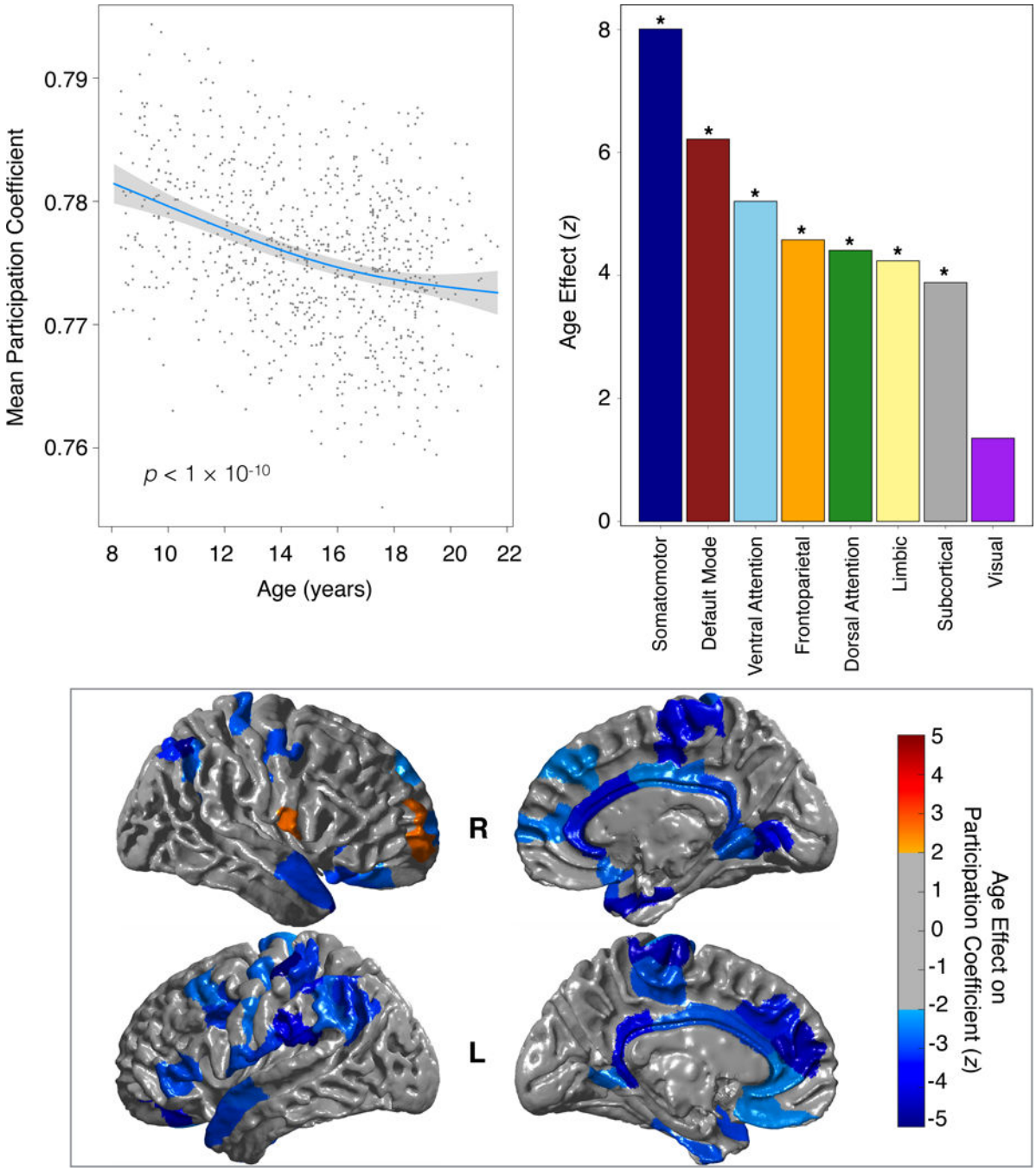

Figure 3. Structural brain network modules become increasingly segregated with age

Modular segregation was quantified as the mean participation coefficient across all network nodes, with lower values indicating more segregation. (**A**) Mean participation coefficient values declined significantly with age. (**B**) Modular segregation is differentially distributed across functional systems. Age-related modular segregation is most robust in the somatomotor and default mode systems, but also present in other networks. (**C**) Age-related changes in participation coefficient provide convergent results for individual nodes, and demonstrate widespread declines with age, particularly within default mode regions such as

Author Manuscript Author Manuscript Author Manuscript Author Manuscript

the posterior cingulate. Two exceptions to this overall trend were the right rostral frontal gyrus and frontal operculum, where participation coefficient increased with age. Blue line represents the best fit from a general additive model; shaded area indicates 95% confidence interval. Color palette represents *z*-transformed *p*-values from a general additive model. Images are thresholded to control for multiple comparisons using the False Discovery Rate ($q<0.05$). *indicates $p<0.001$. See also Figures S1, S3, S6, S7, and Table S1.

Author Manuscript Author Manuscript Author Manuscript Author Manuscript

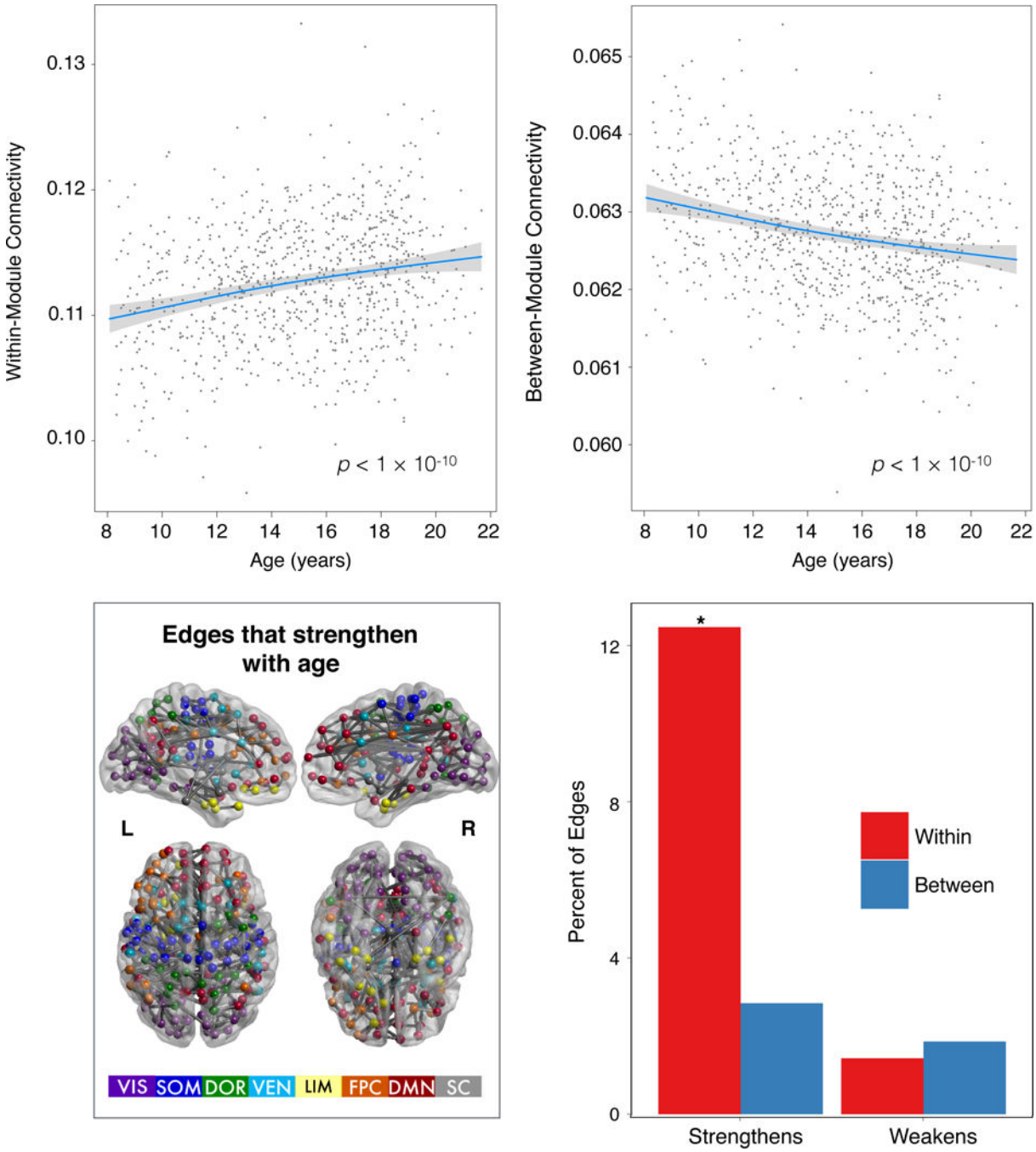

Figure 4. Modular segregation is driven by a combination of both enhanced within-module connectivity and reduced between-module connectivity

(**A**) Average strength of within-module connectivity increases with age. (**B**) Between-module connectivity decreases across development. (**C**) Convergent effects are seen at the level of individual graph edges (image thresholded using Bonferroni corrected p<0.05 for clarity). (**D**) A higher percentage of within-module connections (red) strengthen with age than expected by chance. * indicates p<0.001. See also Figure S1.

Author Manuscript
Author Manuscript
Author Manuscript
Author Manuscript

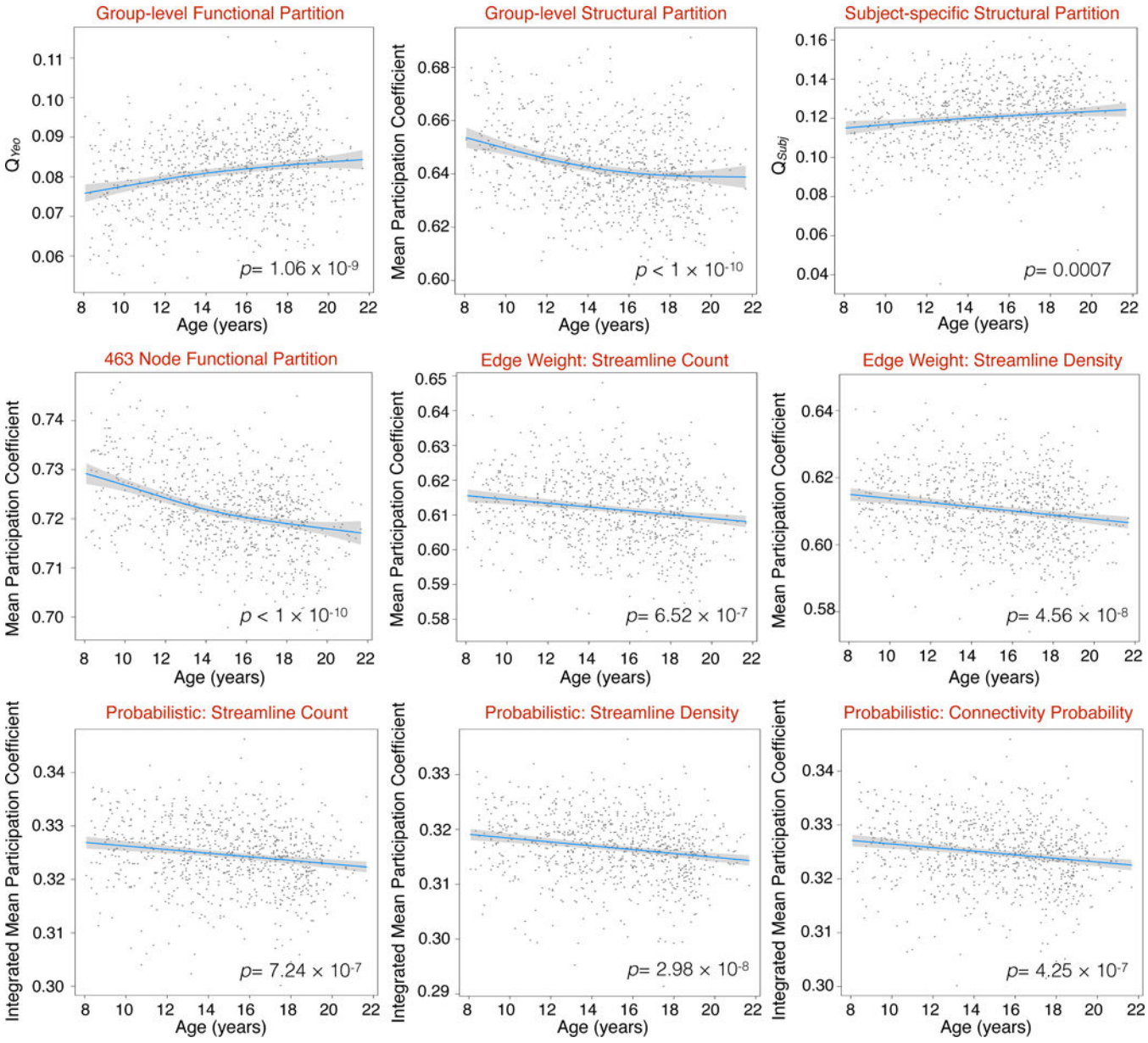

Figure 5. Results are robust to methodological choices

Regardless of specific processing decisions, an increase in modular segregation with age was observed. (**A**) Convergent findings result when using an index of the modularity quality for the Yeo partition [6], where higher *Q* indicates more segregated modules. (**B**) When using a group-level structural partition, modular segregation (mean participation coefficient) decreases with age. (**C**) Modularity quality of subject-level connectivity matrices also increases with age. (**D**) Results remain unaffected when a higher-dimensional parcellation is used (n=463 nodes), (**E**) when streamline count is used instead of FA as an edge weight, and (**F**) when normalized streamline density is used as the edge weight. For brain networks derived from probabilistic tractography, mean participation coefficients were integrated across a wide density range (5–60%). We observed an age-related increase in modular segregation when edge weights were defined by (**G**) probabilistic streamline count, (**H**)

probabilistic streamline density, and (**I**) inter-regional connectivity probability. Lower participation coefficient indicates more segregated modules. Blue line represents the best fit from a general additive model; shaded area indicates 95% confidence interval. See also Figures S1, S2, S4, and S5.

Author Manuscript Author Manuscript Author Manuscript Author Manuscript

Author Manuscript Author Manuscript Author Manuscript Author Manuscript

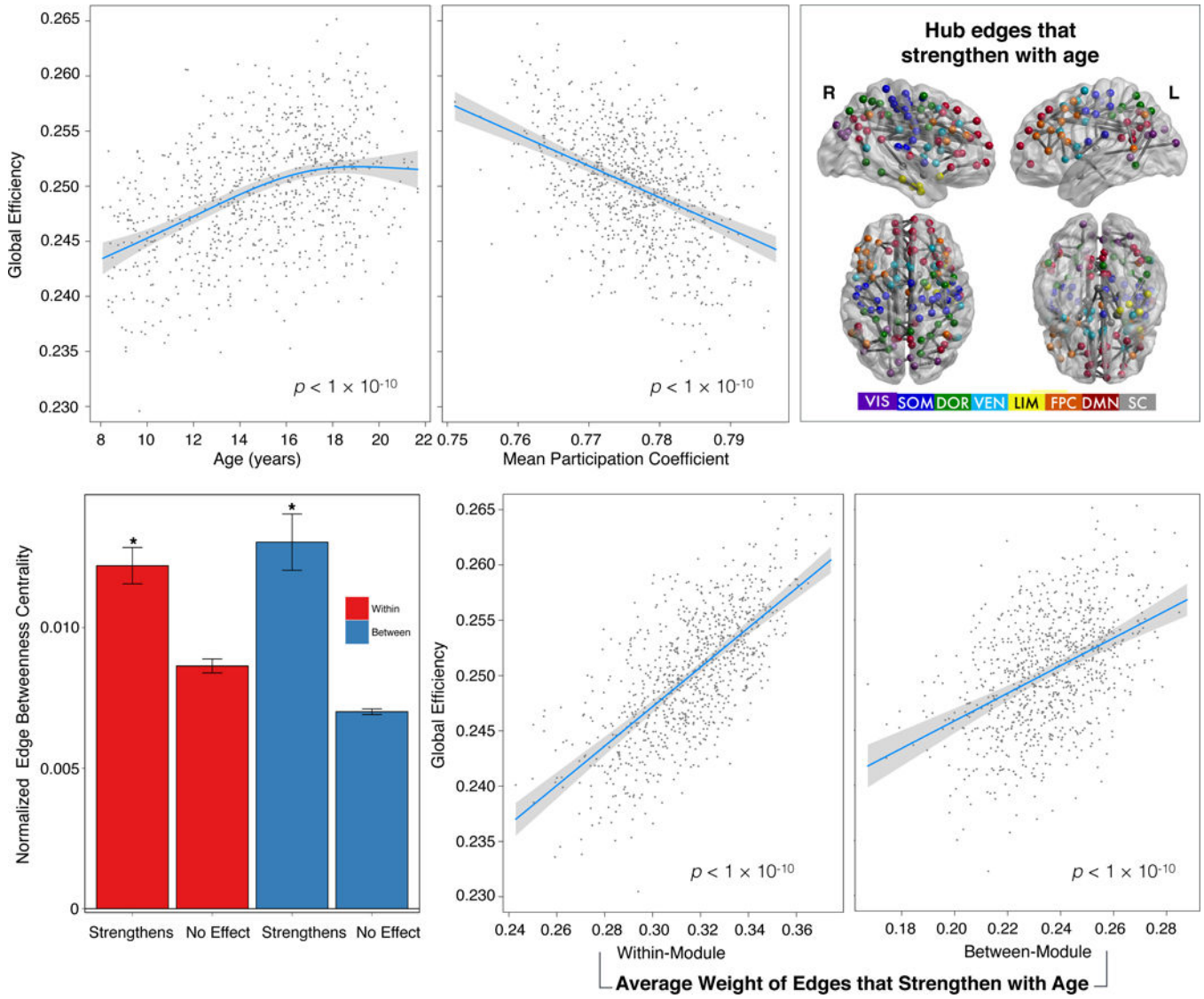

Figure 6. Modular segregation promotes global network efficiency, and is driven by developmental strengthening of specific hub edges

(**A**) Replicating prior work, global network efficiency increases with age. (**B**) While controlling for age, lower mean participation coefficient is associated with greater network efficiency, indicating a positive association between modular segregation and network efficiency. (**C**) Connections that strengthen with age are enriched for hub edges (47%). Hub edges are defined as connections in the top quartile of edge betweenness centrality, which quantifies how often a given edge lies on the shortest path between nodes and thus facilitates global efficiency. Image thresholded using Bonferroni corrected $p<0.05$ for clarity. (**D**) Both within-module and between-module connections that strengthen with age have higher edge betweenness centrality than expected by chance. The average weight of (**E**) within-module and (**F**) between-module edges that strengthen with age are positively associated with global efficiency. Blue line represents the best fit from a general additive model, shaded area indicates 95% confidence interval; * indicates $p<0.001$. Error bar represents standard error of the mean. See also Figure S1.

Author Manuscript Author Manuscript Author Manuscript Author Manuscript

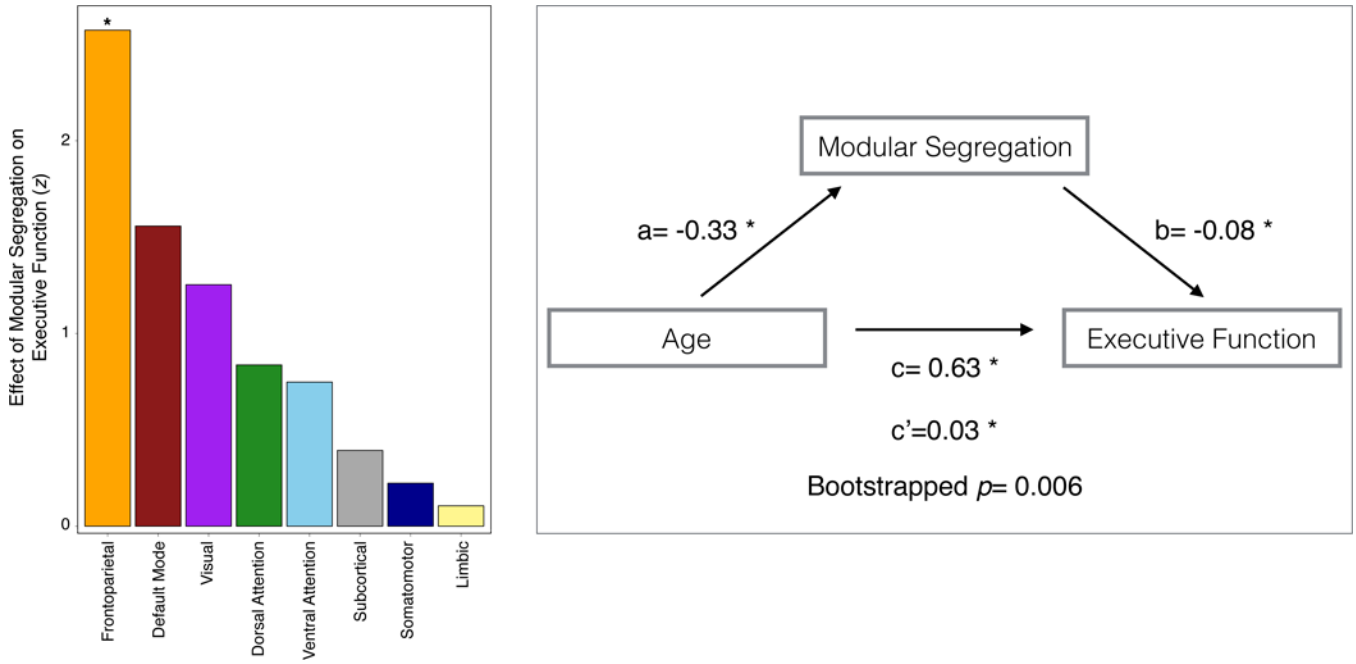

Figure 7. Segregation of structural modules mediates the development of executive function in youth

(**A**) While controlling for age, greater modular segregation in the frontoparietal control network is uniquely associated with better executive performance (n=880). (**B**) Segregation of structural modules mediates the improvement of executive function with age. Mediation results shown as standardized regression coefficients. Significance of indirect effect (c'=0.03) was assessed using bootstrapped confidence intervals [0.008–0.045]. The asterisk (*) indicates p<0.01. See also Figure S1.

Author Manuscript Author Manuscript Author Manuscript Author Manuscript

KEY RESOURCES TABLE

REAGENT or RESOURCE	SOURCE	IDENTIFIER
Deposited Data		
Philadelphia Neurodevelopmental Cohort	[32]	https://www.ncbi.nlm.nih.gov/projects/gap/cgi-bin/study.cgi?study_id=phs000607.v1.p1
Software and Algorithms		
MATLAB R2014B	MathWorks, Natick, MA, USA	http://www.mathworks.com/
FSL 5.0.5	Oxford Centre for Functional MRI of the Brain, Oxford, UK	https://fsl.fmrib.ox.ac.uk/fsl/fslwiki
FreeSurfer 5.3	Massachusetts General Hospital, Harvard Medical School, MA, USA	http://surfer.nmr.mgh.harvard.edu/
DSI Studio	University of Pittsburgh, PA, USA	http://dsi-studio.labsolver.org/
Brain Connectivity Toolbox	[88]	https://sites.google.com/site/bctnet/
genlouvain	University of Northern Carolina, NetWiki	http://netwiki.amath.unc.edu/GenLouvain/GenLouvain
Other		
3 Tesla Siemens TIM Trio whole-body MRI	Siemens Medical Solutions USA, Inc, Malvern, PA, USA	https://usa.healt.hcare.siemens.com/